Benemérita Universidad Autónoma de Puebla

Facultad de Ciencias Físico-Matemáticas

Bounds on Lorentz-violating Yukawa couplings via lepton electromagnetic moments

Tesis presentada al

Posgrado en Física

como requisito parcial para la obtención del grado de

Doctor en Física

por

M.C. Mónica Salinas Ibañez

asesorada por

Dr. Héctor Novales Sánchez

Dr. J.Jesús Toscano Chávez

Puebla, Pue.

Diciembre 2021

Benemérita Universidad Autónoma de Puebla

Facultad de Ciencias Físico-Matemáticas

Bounds on Lorentz-violating Yukawa couplings via lepton electromagnetic moments

Tesis presentada al

Posgrado en Física

como requisito parcial para la obtención del grado de

Doctor en Física

por

M.C. Mónica Salinas Ibañez

asesorada por

Dr. Héctor Novales Sánchez

Dr. J.Jesús Toscano Chávez

Puebla, Pue.

Diciembre 2021

Título: Bounds on Lorentz-violating Yukawa couplings via lepton electromagnetic moments

Estudiante: M.C. Mónica Salinas Ibañez

COMITÉ

_____

Dr. Gerardo Francisco Torres del Castillo

Presidente

_____

Dr. Carlos Gerardo Honorato Méndez

Secretario

_____

Dr. Gilberto Tavares Velasco

Vocal

_____

Dr. Héctor Novales Sánchez

Dr. J.Jesús Toscano Chávez

Asesor

Contents

Abstract

The following investigation has been performed within the Lorentz and CPT violating Standard Model Extension, an effective field theory that sets a quite general framework to quantify, at relatively low energies, effects to be expected from a higher energy formulation incorporating violation of Lorentz invariance. The discussion has been restricted to couplings occurring in the Yukawa sector of the renormalizable part of the Standard Model Extension studying the contributions to anomalous magnetic moment (AMM) and electric dipole moment (EDM) of charged leptons and nucleons which are invariant under Lorentz particle transformations, these effects are calculated and discussed. In a perturbative approach, treating Lorentz violating quadratic lepton couplings as two point insertions in Feynman diagrams, explicit expressions of leading contributions are derived and upper bounds on Lorentz violation coefficients from current data of AMMs and EMDs are estimated. For the lepton analysis, two scenarios involving these coefficients are examined. The scenario of two point insertions preserving lepton flavor, the bound on the electron EDM yields limits as stringent as 10^{-27}, whereas muon and tau lepton have bounds as restrictive as 10^{-14} and 10^{-5}, respectively. A scenario defined by the assumption that Lorentz violating Yukawa couplings are Hermitian leads to less stringent bounds provided by the muon AMM, which is as restrictive as 10^{-14}. We also estimate contributions of Lorentz violating parameters of quarks, at first order, by analyzing the AMM and EDM of nucleons; bounds as stringent as 10^{-12} have been established for this case.

Introduction

Lorentz symmetry has been an essential part of all fundamental theories of nature since its discovery in 1905 [1–3]. It becomes extremely important when the regime of validity of these theories extends to high and relativistic energies. Lorentz symmetry is thus an integral part of the two pillars of modern physics: the Standard Model (SM) of particle physics and General Relativity. Of course, the recognition of the significance of Lorentz symmetry stems from Einstein's insights, which resulted in a radical shift in our understanding of space and time, as summarized in his theories of special and general relativity [4,5].

Lorentz transformations are mathematical operations used to connect physical observations made in reference frames that have relative velocities and different orientations between them, i.e. inertial reference frames. These operations are referred to as boosts and rotations. Rotations, of course, account for changes in angle between reference frames, whereas boosts connect a frame that moves with a constant velocity with respect to another frame. Lorentz symmetry states that physical laws should appear the same in all inertial reference frames.

A Lorentz transformation can be defined as one that leaves the spacetime interval $ds^2 = dx_\mu dx^\mu$ invariant (the Einstein summation convention is employed). For a four vector like x^μ, a Lorentz transformation is implemented by a matrix $\Lambda^\mu{}_\nu$, which transforms x^μ to a new reference frame: $x^\mu \to x'^\mu = \Lambda^\mu{}_\nu x^\nu$. If ds^2 is invariant, then the defining property of a Lorentz transformation becomes

$$g_{\mu\nu}\Lambda^\mu{}_\alpha \Lambda^\nu{}_\beta = g_{\alpha\beta}, \tag{1}$$

where $g_{\mu\nu}$ is the Minkowski metric.

At low energies, effects of Lorentz and CPT symmetry violation can be described in a model independent way by the so called Standard Model Extension (SME), which is an effective field theory that contains General Relativity and the SM [6, 7], the last one is the theory that remains our best theoretical description of fundamental physics nowadays [8]. Lorentz symmetry is considered a low energy manifestation of an underlying theory operating at some very high energy scale, perhaps of the order of the Planck mass ($M_p \approx 10^{19}$GeV [9]). Invariance under spacetime and gauge transformations have received much attention in model building. While Lorentz symmetry is a conventional assumption in beyond SM contexts, Planck scale physical formulations, such as string theory and non commutative

field theory, can spontaneously break it [10–14]. This yields Lorentz non conserving physical phenomena which may manifest as tiny measurable effects at current experimental sensitivity. Some theories related to quantum gravity suggest that Lorentz symmetry invariance (LI) may not be exact and breaks down at high energies [15].

Lorentz violation (LV) has not been ever observed, but there is a catalog of SME coefficients constraints updated every year [16]. We do not know which place is the best to introduce this kind of new physics, it seems to be suitable to follow an effective Lagrangian approach [10, 17], distinguished for being model independent. Decades ago, an effective Lagrangian description of Lorentz symmetry non conservation known as the Lorentz and CPT violating SM extension was formulated [18, 19]. The SME induces unconventional phenomena such as vacuum birefringence [20, 21], vacuum Čerenkov radiation [22, 27], oscillations of massless neutrinos [28–31], exotic electromagnetic properties of SM particles [32, 33], and violations of standard theorems of Quantum Field Theory [34, 35]. One characteristic of the SME is that dynamic variables and gauge symmetry group are the same as those of the SM, the key element being a large set of coefficients characterized by fully contracted spacetime indices within Lagrangian terms and which transform as tensors under observer Lorentz transformations [18, 19]. However, these tensor coefficients, which define preferred directions in spacetime, are invariant under particle Lorentz transformations, so they do not preserve Lorentz symmetry.

The SME Lorentz violating Lagrangian terms are classified into two categories, according to whether they are power counting renormalizable or not [35–40]. The full set of renormalizable SME terms define the so called minimal SME (mSME). The bound estimations of mSME coefficients have become the main objective of the present phenomenological investigation about Lorentz violation effects on the AMMs, a_A, and EDMs, d_A, of charged leptons l_A, with $A = e, \mu, \tau$ labeling lepton flavors. It is important to emphasize that external fermion lines are always taken to preserve lepton flavor. As a result, our calculations of SME contributions to AMMs and EDMs only include diagonal electromagnetic moments.

We consider the general Lorentz violating extension of the minimal $SU(3) \times SU(2) \times U(1)$ SM using CPT even terms. We will focus on a Yukawa sector extended by renormalizable Lorentz violating interactions which have gauge structure. Lorentz violation from these interactions is introduced in the Feynman diagrams through electromagnetic vertexes with two and three point insertions and contributions to electromagnetic form factors are generated by one loop Feynman diagrams with virtual Higgs or Z bosons and photon lines. The last one dominates over the others. The current AMMs and EDMs experimental data reports are employed to estimate upper bounds on mSME coefficients.

Two scenarios are considered for the analysis: in the first one, those mSME parameters given by lepton flavor non conserving two point insertions, inside the loop, are assumed to be quite small in comparison to those that preserve the virtual lepton flavor, leaving optimal conditions to bound Lorentz violation coefficients of order 10^{-27} from the EDM of the electron, and limits as restrictive as 10^{-14} and

10^{-5} if constraints on the muon and the tau lepton electromagnetic moments are considered, respectively. Another scenario, considering the assumption that Yukawa like related couplings are Hermitian, also gives rise to bounds on mSME coefficients. In this scenario, the analysis of mSME contributions and their comparison with current experimental bounds on electromagnetic moments of charged leptons determine upper limits on the impact of Lorentz violating coefficients as stringent as 10^{-15}, which, specifically, are imposed by the AMM of the muon. In this scenario, mSME contributions to EDM absent.

Other analyses we include are related to the electromagnetic moments (EMMs) of nucleons. First, we compute the electromagnetic contributions of the quarks and use specific relationships to calculate the proton AMM and neutron EDM. High sensitivity measurements of these proton and neutron EMMs then yield constraints on SME coefficients, with bounds as restrictive as 10^{-12}.

The following is the structure of the thesis. In Chapter 1, the Lorentz and CPT symmetry violation theories are presented, as well as the observer and particle Lorentz transformations and the experimental test for LI violation. The second chapter discusses SME, with focus on the renormalizable extension, the theoretical framework required for the phenomenological calculation is discussed, and an analytical calculation of the electromagnetic vertex $A_\mu l_A l_A$ at one loop is performed. In Chapter 3, there are numerical estimates and a discussion of the results. The Lorentz violation in nucleon electromagnetic moments is examined in Chapter 4. Finally, in Chapter 5, there is a summary and conclusions.

0.1   Publications related to this thesis

- J. Alfonso Ahuatzi-Avendaño, Javier Montaño, Héctor Novales-Sánchez, Mónica Salinas, and J. Jesús Toscano, *Bounds on Lorentz-violating Yukawa couplings via lepton electromagnetic moments*, Phys. Rev. D **103**, 055003 – Published 2 March 2021; Erratum Phys. Rev. D **104**, 119902 (2021).

- Javier Montaño-Domínguez, Héctor Novales-Sánchez, Mónica Salinas, and J. Jesús Toscano, *Lorentz violation in nucleon electromagnetic moments*, e-Print: 2107.12444.

Chapter 1

Lorentz and CPT symmetry

The concept of symmetry is one of the most important elements in physics, as it is closely related to the conservation of quantities such as charge, energy, momentum, and so on. However, the question of when symmetry is broken is also of great importance. For example, the breaking of electroweak symmetry gives rise to the mass of SM particles.

Albert Einstein was the first physicist to use the concept of Lorentz symmetry to describe the behavior of the universe. He assumed that special relativity is governed by Lorentz Symmetry and postulated that the laws of physics are the same for all inertial observers. An inertial observer can be anyone, who has a system of calibrated clocks and rulers, located in a non accelerated reference frame with respect to an inertial frame. When these kinds of observers move relative to each other, the measurements of time and length intervals are different of each other. The generalization of these differences is described by a set of equations called Lorentz transformations.

Spacetime symmetries have a particularly fundamental weight in physics, there are two types. The Lorentz transformations are well-known continuous spacetime symmetries that include global translations in space and time as well as boosts and rotations. CPT involves the discrete space- and time-inversions, P, T and the charge conjugation operation on the fields, C. C can be associated with the exchange of particles and antiparticles, P with the reflection of all three spatial coordinate (e.g., $\vec{r} \rightarrow -\vec{r}$) and T with the inversion of the time coordinates (e.g., $t \rightarrow -t$). Lorentz and CPT symmetries are closely related, a fact of great importance for experimental studies of spacetime symmetries.

In order to interpret and study the symmetry properties of a model, it is crucial to consider the correct type of transformation. In physics, coordinate transformations are generally inappropriate, because coordinates, while used to describe observables and relationships to each other, are merely a labeling of spacetime points that is largely arbitrary and without actual physical meaning. In other words, a physical phenomenon should be independent of the chosen coordinate system and observer. Coordinate independence is also called observer invariance. In contrast, the study of how transformed dynamical

variables continue to satisfy the same equation is of greater importance. This case corresponds to the actual experimental situation where measurements are compared before and after the transformation of the device (not the observer). Such types of physical transformations are called particle transformations. In this context, the CPT transformation of the coordinate system is not sufficient to study the properties of a particular model, since the transformations must be applied according to transformation of the experimental setup.

Invariance under Lorentz and CPT symmetry is a fundamental part of quantum field theory and General Relativity. This is the main reason why physicists have been unwilling to consider violations of these symmetries. There are two reasons to consider the possibility that Lorentz symmetry is not an exact symmetry of nature [41]. On the theoretical side, there are theories of quantum gravity that include violation of Lorentz invariance as a possible effect, for example, non commutative geometry [42], String theory [43], loop quantum gravity [44], theories with emergent gauge bosons [45,46], and emergent gravity [47]. On the experimental and phenomenological side, effective field theories of low energy with violation of Lorentz invariance have been studied. The Lorentz symmetry violation effects can be estimated using phenomenology and compared with the experiments in order to constrain the LV parameters. For example, the so called SME has attracted much interest to test Lorentz and CPT symmetries. This model contains all possible terms in which the SM fields are coupled in a Lorentz covariant manner to constant tensor coefficients. The value of these coefficients can in principle be measured or bound by experiments or phenomenological results, which is the goal of this work.

CPT invariance is a topic closely related to Lorentz invariance. The CPT theorem [48] states that any Lorentz invariant local quantum field theory with Hermitian Hamiltonian must have CPT symmetry. In contrast, it can be shown [49] that any unitary interacting theory violating CPT necessarily violates Lorentz invariance. This means that we cannot have CPT violation without Lorentz symmetry violation, but violation of Lorentz invariance while preserving CPT symmetry is a possibility.

1.1 Observer and particle Lorentz transformations

Physics must be described in a coordinate independent manner. That is, if an experiment has a predetermined outcome, any two observers should arrive at the same conclusion. In other words, whether or not Lorentz invariance is violated, nature should not be concerned with the observer or the coordinates used to describe a physical process. As a result, the SME Lagrangian, and thus all physical observables that can be derived from it, is observer Lorentz invariant. This is what we mean by observer Lorentz transformations: they are simply changes in coordinates.

Passive (observer) Lorentz transformation should be contrasted with active (particle) Lorentz transformation. When we talk about the breakdown of Lorentz invariance, we actually mean the breakdown

of active Lorentz transformation invariance. The SME Lagrangian introduces the breakdown of Lorentz invariance via tensor coefficients coupled to operators built out of SM fields. Here is an example:

$$\mathcal{L} = ic_{\mu\nu}\bar{\psi}\gamma^\mu\partial^\nu\psi, \tag{1.1}$$

where $c_{\mu\nu}$ is the Lorentz violating coefficient. All Lorentz violating coefficients in the SME can be viewed as constant valued background fields. When using an **observer Lorentz transformation**, all quantities, including background fields, are transformed. In the case of Eq. (1.1), obtaining

$$ic_{\mu\nu}\bar{\psi}\gamma^\mu\partial^\nu\psi \rightarrow \Lambda_\mu{}^\rho\Lambda_\nu{}^\sigma\Lambda^\mu{}_\lambda\Lambda^\nu{}_\kappa ic_{\rho\sigma}\bar{\psi}\gamma^\lambda\partial^\kappa\psi = ic_{\mu\nu}\bar{\psi}\gamma^\mu\partial^\nu\psi, \tag{1.2}$$

where $\Lambda_\nu{}^\sigma$ represents a Lorentz transformation, for which Eq. (1) holds by definition. As a result, that all Lorentz indices are contracted implies observer Lorentz invariance. When building the SME, one demands that all the terms in the Lagrangian are invariant under observer Lorentz transformations, which translates into the fact that all Lorentz indices should be contracted. A **particle Lorentz transformation**, on the other hand, transforms all quantities except the background fields, giving the following

$$ic_{\mu\nu}\bar{\psi}\gamma^\mu\partial^\nu\psi \rightarrow \Lambda^\mu{}_\lambda\Lambda^\nu{}_\kappa ic_{\mu\nu}\bar{\psi}\gamma^\lambda\partial^\kappa\psi. \tag{1.3}$$

This corresponds to physically boosting or rotating the experiment with respect to the background. This occurs, for example, when the Earth moves through space and the experiment moves with it. As seen from the laboratory frame, the values of $c_{\mu\nu}$ will change as the Earth rotates. These values will thus oscillate with the frequency rotation of the Earth (or proportional to that frequency).

According to the previous explanation, there is an example, illustrating two ways to perform Lorentz transformations over the magnetic moment $\vec{\mu}$ of some particle:
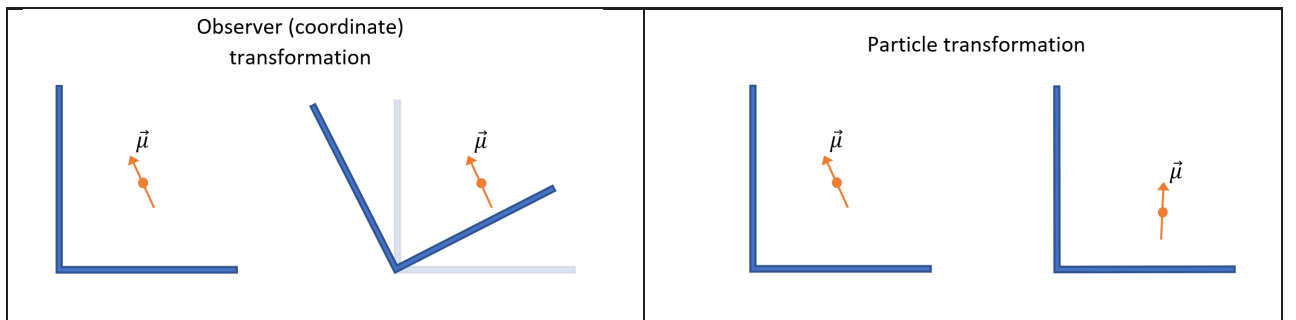
Figure 1.1: Magnetic moment, $\vec{\mu}$, of a particle. Observer and particle transformation. LI symmetry occurs.

The rotation of the reference system is represented by observer transformation (the coordinates are transformed). Passive transformation is the term used to refer to it. This type of invariance has nothing to do with physics. A particle transformation, on the other hand, represents a rotation of the particle; this is known as active transformation, and it actually changes the physical position of the particle. The

physical symmetry of the system is represented by invariance with respect to these transformations.

Both transformations are inversely related in the vacuum, when LI occurs, which means that rotating the reference system by *theta* is equivalent to rotating the particle by $-theta$, as we can deduce from Fig. (1.1).

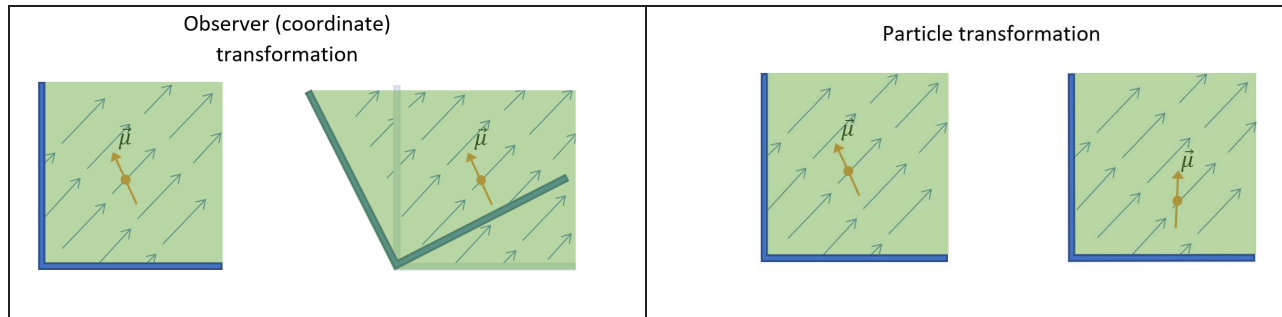
Figure 1.2: Magnetic moment, $\vec{\mu}$, of a particle with background field. Observer and particle transformation

Figure (1.2) illustrates that in the presence of a background field $\vec{B}$, the system is invariant under observer transformations. For example, if we focus in the interaction $U = -\vec{\mu} \cdot \vec{B}$, we observe that it remains invariant under coordinate transformation, leaving the interaction rotationally invariant. When a particle transformation is performed, however, the system is physically distinguishable from its transformed version because of the existence of the background field can be inferred from the experiment. We can deduce that the field $\vec{B}$ breaks the symmetry by specifying a preferred direction.

For example, the following Lorentz violating SME terms

$$\mathcal{L}_{LV} = -a_\mu \bar{\psi} \gamma^\mu \psi - b_\mu \bar{\psi} \gamma^\mu \gamma^5 \psi - \frac{1}{4}(k_f)_{\mu\nu\lambda\sigma} F^{\mu\nu} F^{\lambda\sigma}, \tag{1.4}$$

are built from SM fields that have been properly contracted with coefficients to form observer scalars. These coefficients act as background fields, producing observable effects that can be investigated in experiments [50–52].

1.2 Effective field theory with Lorentz violation symmetry

The SME [53] is an effective field theory satisfying: i) General Relativity and the Standard Model, ii) scalar terms obtained by the contraction of operators for the violation of Lorentz symmetry with tensor coefficients, and iii) possible additional requirements such as gauge invariance and renormalizability.

In principle, the SME includes terms of arbitrary mass dimension, but the requirement of renormalizability focuses on terms of dimension four, which is called the minimal SME. The mSME has a finite number of Lorentz invariance violation parameters, while the number of these parameters in the full

SME is essentially unbounded.

The considerations stated by Kostelecký in Ref. [54] can be summarized to motivate the employment of the SME instead of some of the other approaches to Lorentz violation. He claims that a method for investigating the loss of Lorentz symmetry should

- *Observer coordinate independence*: Any event should be independent of the observer Lorentz transformation, i.e. it is not about the coordinates of the observer, it must to describe the same physical situation.

- *Realism*: The theory must incorporate known physics while allowing for the parametrization of the effects of the Lorentz symmetry violation.

- *Generality*: The framework should be as general as possible.

1.3 Lorentz invariance violation experimental tests

It is important to remember that there is no single best test of Lorentz symmetry. It is possible for one type of particle in the SM to have interactions that violate Lorentz symmetry while other particles may not violate LI at all, an exhaustive investigation of Lorentz violation requires a large number of experiments to probe every particle sector. The current limits on Lorentz violating effects are derived from both terrestrial and astrophysical experiments [55].

1.3.1 Terrestrial constraints

Photons are used in the most famous tests of Lorentz symmetry, the Michelson-Morley experiments [56]. A light beam is divided into two beams that travel perpendicularly to each other, which are reflected by mirrors, and are then recombined to form an interference pattern. The produced pattern is determined by the different lengths of the two paths. As the interferometer is rotated, the researchers look for a change in this pattern. Because it is sensitive to any dependence of the speed of light or direction in space, this effectively serves as a test of Lorentz symmetry. Kennedy-Thorndike experiments, which use an interferometer that is fixed in the laboratory, are closely related to Michelson-Morley experiments. Researchers are looking for a change in the interference pattern over time as a result of the Earth's motion around the Sun. Because it is sensitive to any variation of the speed of light, this serves as a test of Lorentz symmetry. Rotation invariance is investigated in Michelson-Morley experiments looking for anisotropy in the speed of light, whereas boost invariance is investigated in Kennedy-Thorndike experiments [57].

Nature has proven to be LI to a very high degree. Therefore, looking for deviations from this symmetry at low energies, described by the renormalizable terms in EFT based approach, requires very high precision, and hence Earth based experiments. Among the most relevant experiments, we can find:

- In 2003, John Lipa and colleagues described the findings of an experiment designed to look for spacetime anisotropy terms that could exist as a result of Lorentz violations. They use a simple configuration consisting of a pair of cylindrical microwave cavity resonators operating in radial modes with their axes aligned in the east-west direction and optimally at 45 degrees from the Earth's axis. Because of the radial nature of the resonators, this apparatus will have a different sensitivity to the coefficients of the Lorentz violating terms than an optical cavity experiment [58].

- Achim Peters and colleagues compared the resonant frequencies of two orthogonal resonators made of crystalline sapphire. They presented the results of the most sensitive Michelson-Morley style frequency comparison experiment performed to date. They used a year of data to set new bounds on the nine possible rotational and boost isotropies of the speed of light, with the results expressed as constraints on coefficients of the SME, finding no significant violations of Lorentz symmetry [59].

- Peter Wolf and colleagues at the Observatoire de Paris compared the frequencies of a cryogenic sapphire oscillator and a hydrogen maser to set new constraints on a possible violation of Lorentz invariance. The difference in the sensitivities of the crystal and the hydrogen maser would provide a Lorentz violating signal in this case. These experiments demonstrated that for a variety of different SME parameters in the photon sector, any violation of Lorentz symmetry must be less than 1 part in 10^{11} [60].

- A Penning trap is a combination of static magnetic and electric fields that can keep a charged particle localized within the trap for extremely long periods of time [61]. A trapped particle can move in a variety of directions. The cyclotron motion in a magnetic field and Larmor precession due to spin are the two motions relevant for Lorentz violation tests. The ratio of the recession frequency ω_s to the cyclotron frequency ω_c is given by

$$\omega_s/\omega_c = g/2,$$

where g is the g-factor of the charged particle. The energy levels for fermions are given by $E_n^s = n\omega_c + s\omega_s$ where n is an integer and $s = \pm 1/2$. For electron and positron, where $g \approx 2$, the state $(n, s = -1/2)$ is almost degenerate with the state $(n-1, s = +1/2)$. The degeneracy breaking is caused solely by the electron's AMM and is commonly denoted by $\omega_a = \omega_s - \omega_c$. By introducing a small oscillating magnetic field into the trap, it is possible to induce transitions between these nearly degenerate energy states and determine the value of ω_a very precisely. The primary application of ω_a measurements is that they provide a very precise value of $g - 2$. These measurements, however, provide good tests of CPT and Lorentz invariance because of their precision."

- For clock comparison experiments, two atomic transition frequencies are usually placed at some point in space. As the clocks move, they pick out different Lorentz violating tensor components in the minimal SME, resulting in a sidereal drift between the two clocks. The difference in clock frequencies can be measured over long periods of time, yielding extremely high precision limits on the amount of drift and thus the mSME parameters. It should be noted that this method is only feasible if the clocks are made of different materials or have different orientations. The best overall limit comes from a $^3He/^{129}Xe$ maser system in the neutron sector of the mSME. In the experiment, the frequencies of helium and xenon masers operating within the same cavity are compared. The energy level corrections in these atoms are highly sensitive to how the neutrons within the nuclei are oriented with respect to the background SME coefficients. As the Earth rotates, these orientations change, and the small difference between the helium and xenon frequencies changes with time. Clock comparison experiments, in other words, constrain protons and neutrons' parameters [62, 63].

- Experiments with a spin polarized torsion pendulum provided the tightest bounds on Lorentz violation for the electron. This device is made up of a torus of alternating magnetic materials chosen in such a way that the torus has a massive net spin aligned electron spins, but produces no magnetic field. As a result, it can be used to measure anomalous spin couplings in the absence of the usual magnetic dipole effects. The pendulum is suspended from a rotating turntable, causing the collective motion of the electron spins in relation to the background SME coefficients to produce a small but detectable torque. Using this experiment, Adelberger and Heckel achieved Lorentz violation sensitivities for the electron of one part in 10^{29} [64].

- Muon experiments open up a new window into the lepton sector of the mSME. If the mSME coefficients are to be small, there must be some small energy scale suppressing the Lorentz violating coefficients. There are only a few small scales available, namely particle masses or a symmetry breaking scale. If we assume the scale is particle mass, then muon based experiments would have a signal at least 10^2 times larger than equivalent electron experiments due to the larger mass of the muon. Of course, because muons are unstable, experiments are inherently more difficult [65].

  The muon sector is constrained by two primary experiments. To begin, muonium spin transitions (μ^+e^-). Despite the fact that muonium is a muon electron system, the muon sector of the mSME can be isolated by immersing the muonium to a strong magnetic field and looking for a specific frequency resonance that corresponds to muon spin flips. The sidereal variation of this transition frequency is then tracked, resulting in a Lorentz violation symmetry coefficient limit of the order $\approx 10^{-22}m_\mu$ [65].

  The second muon experiment that yields strong limits is the μ^-/μ^+ $g-2$ test [66–68]. In this

study, relativistic μ^- (or μ^+) are injected into a storage ring and allowed to decay. The deposit rate of the decay products along the detector is sensitive to the evolution of the muon's spin, which is a function of $g-2$ for the muon. Lorentz violation alters this evolution equation, and thus these types of $g-2$ experiments can constrain the mSME. The muon $g-2$ experiment yields two types of bounds: a direct comparison between the $g-2$ factors for μ^- and μ^+, which limits the CPT violating coefficient $< 10^{-22}$, and the analysis of sidereal variations involving only one of the μ^- and μ^+ at the current sensitivity in [68] could bound the CPT violating coefficient at the level of 10^{-25} [66].

- Because the constraints on various parameters of the mSME are so tight, considering loop effects can yield interesting indirect constraints on unmeasured sectors. Such an approach is taken in, which considers loop corrections to mSME coefficients caused by Lorentz violation in the Higgs sector. There are four parameters in the Higgs sector of the mSME that have been bounded. Three of them come from the birefringence constraints on photon propagation, the constraint on all the coefficients are of order 10^{-16}. The other can be derived from the cyclotron frequencies of hydrogen ions and antiprotons and is of order 10^{-13} [69].

1.3.2 Astrophysical observations

Some alternatives to laboratory based experiments make use of light emitted by distant astrophysical sources. Because light travels across vast areas of space, these experiments have much higher precision than the previous ones. The long propagation time can magnify any minor differences in the properties of light, such as wavelength or polarization, caused by Lorentz violation.

- Roman Jackiw and colleagues investigated the experimental limits of Maxwell theory modification, which also involves a mass parameter p_α but respects gauge invariance, rather, Lorentz invariance is violated. The modification entails inserting a Chern-Simons term into the Maxwell-Lagrange density. They investigate the observational effects of the Cherm-Simons term as a parametrization of Lorentz invariance violation, demonstrating that SME parameters that violated CPT symmetry could be tested with a precision of 10^{-42} in measurements of light from distant galaxies [70].

- Kostelecký and Matthew Mewes investigate the implications of the SME for light properties, focusing on the CPT even coefficients for Lorentz violation in the photon sector. They use spectropolarimetry of cosmological sources to obtain Lorentz violation bounds comparable to the best current limits in the fermion sector, with a sensitivity of one part in 10^{32}. By analyzing infrared, visible, and ultraviolet light from distant galaxies, they investigated a Lorentz violating effect that causes the polarization of light to change depending on its wavelength [71].

- In SME with mass dimension five operators, odd in CPT, particles with opposite helicity have slightly different group velocities, implying that the polarization vector of a linearly polarized

wave rotates differently for different photon energies during wave propagation; this phenomenon is known as vacuum birefringence. This effect disrupts the amount of polarization in the wave over long distances. The technique has been used to study a variety of astronomical sources such as Gamma-ray Bursts (GRBs) and Pulsar Wind Nebulae (PWNe). This method produced the strongest constraint on ξ, indicating the strength of the Lorentz violation, in the order of 10^{-10} [72, 73].

- The extra terms in the SME approach can be thought of as extra mass terms, which is why LI violation (LIV) corrections are necessary for threshold processes. Lorentz violation symmetry in efective field theory introduces a rich phenomenology related to threshold reactions, and threshold theorems can be generalized [74, 75]. The various aspects investigated in threshold reaction experiments are as follows:

  - A shift in the energy threshold of existing reactions, which leads to higher thresholds.

  – The possibility of a pair production reaction with unequal emitted momenta.

  – The viability of new, normally forbidden, reactions.

- Because LIV affects synchrotron radiation, effective constraints can be derived by comparing observed and expected synchrotron spectra from astrophysical sources. This technique enables the application of strong constraints to mass dimension four and five LIV operators. With observations of the Crab Nebula, constraints on the lepton sector have been obtained. They compare the data from multiwavelength observations to a complete and self consistent computation of the Crab Nebula's broad band spectrum. They cast constraints on the lepton Lorentz Violation parameters of order 10^{-5} with a 95% confidence level [76–80].

- Electromagnetic Čerenkov radiation in ponderable media has been extensively studied since its discovery in the early 1930s [81, 82]. It occurs when the velocity of a massive charged particle exceeds the phase velocity of light in a medium, rendering the particle unstable to Čerenkov light radiation. In the presence of Lorentz violation, the vacuum acts as a refractive medium for particles whose properties are controlled by the Lorentz violation coefficients [83]. Under these conditions, a particle traveling faster than the speed of light in a vacuum can produce vacuum Čerenkov radiation, which continues until the particle loses enough energy to slow down to less than the speed of light. The observation of high energy particles of various species limits the existence of vacuum Čerenkov radiation and, as a result, limits certain Lorentz violation coefficients in the matter sector [84–89]. Čerenkov radiation is only possible for superluminal particles, which usually occur for only one coefficient sign, so any single coefficient constraint is normally one sided. The best fit of Lorentz violation coefficient is of the order 10^{-23} [90].

1.4   Standard Model Extension

The SME is a low energy effective description of particle physics that incorporates Lorentz violation. The model can be defined as the SM lagrangian plus all additional Lorentz and CPT violating terms involving fields that maintain invariance under observer Lorentz transformations. This invariance ensures that the physics is unaffected by the choice of coordinates. The SME Lagrangian is thus constructed from conventional SM fields, as well as coefficients that characterize the Lorentz violation, which can be viewed as originating from vacuum expectation values of Lorentz tensors in an underlying fundamental theory. The requirements of the derivation impose various constraints on the possible structures of both parts (coefficients and fields). Taken together, these requirements impose significant constraints on the form of terms in the SME. Because the usual SM agrees well with experiment, the additional terms must be small [91].

The coupling coefficient part contains spacetime indices that reflect the properties of the relevant nonzero expectation values from the fundamental theory under observer Lorentz transformations. Although the coupling coefficient is complex, it is constrained by the requirement that the Lagrangian is Hermitian. We will assume that these coefficients are position independent. This implies that the violation is limited to the Lorentz symmetry rather than the full Poincaré symmetry. The preceding supposition has several experimentally useful consequences, including the conservation of energy and momentum. We focus on the renormalizable sector of the theory because it is expected to dominate physics at low energies. Non renormalizable terms, on the other hand, are known to play a significant role at higher energies [92].

Terms of the $\mathcal{T}^{\mu_1,\dots,\mu_n}\mathcal{O}_{\mu_1,\dots,\mu_n}(x)$ form are included in the SME. The Lorentz n-tensors $\mathcal{O}_{\mu_1,\dots,\mu_n}(x)$ are assumed to be SM field dependent and covariantly transform under both particle and observer Lorentz transformations; however, the constants $\mathcal{T}^{\mu_1,\dots,\mu_n}$ covariantly transform under only observer Lorentz transformations [12, 13, 18, 19].

We adhere to the same conventions and notations as in Ref. [19], where the complete mSME Lagrangian was first presented. The Lagrangian is constructed from the SM fields. The left and right handed lepton and quark multiplets are denoted by

$$L_A = \begin{pmatrix} \nu_a \\ l_A \end{pmatrix}_L, \qquad R_A = (l_A)_R,$$

$$Q_A = \begin{pmatrix} u_a \\ d_A \end{pmatrix}_L, \quad U_A = (u_A)_R, \quad D_A = (d_A)_R, \tag{1.5}$$

where A labels the flavor of the leptons: $l_A \equiv (e, \mu, \tau)$, $\nu_A \equiv (\nu_e, \nu_\mu, \nu_\tau)$, $u_A \equiv (u, c, t)$ and $d_A \equiv (d, s, b)$. As customary, we define left handed and right handed fields

$$\psi_L \equiv \frac{1}{2}(1 - \gamma_5)\psi, \qquad \psi_R \equiv \frac{1}{2}(1 + \gamma_5)\psi. \tag{1.6}$$

The complete lagrangian for the Lorentz breaking SME can be decomposed into a sum of terms: SM + terms with LIV. We first provide the lagrangian terms in the $SU(3) \times SU(2) \times U(1)$ SM. The lepton and quark parts are given by

$$\mathcal{L}_{\text{lepton}}^{\text{SM}} = i\bar{L}_A \gamma^\mu D_\mu L_A + i\bar{R}_A \gamma^\mu D_\mu R_A, \tag{1.7a}$$

$$\mathcal{L}_{\text{quark}}^{\text{SM}} = i\bar{Q}_A \gamma^\mu D_\mu Q_A + i\bar{U}_A \gamma^\mu D_\mu U_A + i\bar{D}_A \gamma^\mu D_\mu D_A, \tag{1.7b}$$

where D_μ is the usual covariant derivative. The Higgs Lagrangian is

$$\mathcal{L}_{\text{Higgs}}^{\text{SM}} = (D_\mu \phi)^\dagger D^\mu \phi + \mu^2 \phi^\dagger \phi - \frac{\lambda}{3!}(\phi^\dagger \phi)^2. \tag{1.7c}$$

The gauge part of the SM lagrangian is

$$\mathcal{L}_{\text{gauge}}^{\text{SM}} = -\frac{1}{2}Tr(G_{\mu\nu}G^{\mu\nu}) - \frac{1}{2}Tr(W_{\mu\nu}W^{\mu\nu}) - \frac{1}{4}B_{\mu\nu}B^{\mu\nu}, \tag{1.7d}$$

here, $G_{\mu\nu}$, $W_{\mu\nu}$ and $B_{\mu\nu}$ are the $SU(3)$, $SU(2)$ and $U(1)$ gauge fields, respectively. All about Yukawa terms, responsible for generating the fermion masses, is shown in the next section.

We will now look at the Lorentz violating portion of the mSME Lagrangian. The lepton and quark parts are given by

$$\mathcal{L}_{\text{lepton}}^{\text{LV}} = \bar{L}_A[i(c_L)_{\mu\nu}^{AB}\gamma^\mu D^\nu - (a_L)_\mu^{AB}\gamma^\mu]L_B + \bar{R}_A[i(c_R)_{\mu\nu}^{AB}\gamma^\mu D^\nu - (a_R)_\mu^{AB}\gamma^\mu]R_B, \tag{1.8a}$$

$$\mathcal{L}_{\text{quark}}^{\text{LV}} = \bar{Q}_A[i(c_Q)_{\mu\nu}^{AB}\gamma^\mu D^\nu - (a_Q)_\mu^{AB}\gamma^\mu]Q_B + \bar{U}_A[i(c_U)_{\mu\nu}^{AB}\gamma^\mu D^\nu - (a_U)_\mu^{AB}\gamma^\mu]U_B$$
$$+ \bar{D}_A[i(c_D)_{\mu\nu}^{AB}\gamma^\mu D^\nu - (a_D)_\mu^{AB}\gamma^\mu]D_B, \tag{1.8b}$$

in these equations, the various Lorentz violating couplings coefficients $c_{\mu\nu}$ and a_μ, are understood to be Hermitian in generation space. The c parameters are CPT even and dimensionless and a parameters are CPT odd and have mass dimension one. The c parameters can be assumed to be traceless over the spacetime indices (i.e. $g_{\mu\nu}c^{\mu\nu} = 0$). A non zero trace does not contribute to Lorentz violation and can be absorbed by a standard field normalization.

The following terms can be written for the Higgs part of the Lagrangian:

$$\mathcal{L}_{\text{Higgs}}^{\text{LV}} = \left[\frac{1}{2}(k_{\phi\phi})^{\mu\nu}(D_\mu\phi)^\dagger D_\nu\phi + h.c.\right] - \frac{1}{2}(k_{\phi B})^{\mu\nu}\phi^\dagger \phi B_{\mu\nu}$$
$$- \frac{1}{2}(k_{\phi W})^{\mu\nu}\phi^\dagger W_{\mu\nu}\phi + [i(k_\phi)^\mu \phi^\dagger D_\mu\phi + \text{h.c.}]. \tag{1.8c}$$

Due to the hermiticity of the Lagrangian, the dimensionless coefficient $k_{\phi\phi}$ is real and symmetric, whereas the other coefficients have dimension of mass and must be real and antisymmetric. The only CPT odd parameter is k_ϕ, which has mass dimensions and can be any arbitrary complex number.

The gauge sector has both CPT even and CPT odd contributions. The CPT even ones are

$$\mathcal{L}_{\text{gauge}}^{\text{LV}} = -\frac{1}{2}(k_G)_{\kappa\lambda\mu\nu}Tr(G^{\kappa\lambda}G^{\mu\nu}) - \frac{1}{2}(k_W)_{\kappa\lambda\mu\nu}Tr(W^{\kappa\lambda}W^{\mu\nu}) - \frac{1}{4}(k_B)_{\kappa\lambda\mu\nu}B^{\kappa\lambda}B^{\mu\nu}, \qquad (1.8\text{d})$$

All of the parameters in this equation are dimensionless and real. They possess Riemann tensor symmetries and a vanishing double trace (since it does not violate Lorentz symmetry). The CPT odd terms are excluded because they cause instabilities in the minimal theory. They are all associated with negative energy contributions, and one of them would directly generate a linear instability in the potential.

It is important to remember that not all the parameters in the mSME are observable in all physical processes. This is demonstrated at the Lagrangian level by the fact that some parameters can be removed from the Lagrangian via field redefinition. The removable parameters cannot appear in physical observables because the physics should be invariant under such field redefinition. A field redefinition must include the associated coupling coefficient in order to eliminate a Lorentz breaking term. When derivative couplings are involved, field redefinition may also include spacetime position variables. Ref. [93] contains an in depth discussion of this topic.

Linear phase redefinition and linear normalization redefinition are two processes that we have found to be particularly useful. Some terms involving the coefficients $a_{L,R,Q,U,D}$, for example, can be eliminated using position dependent field phase redefinition, as described in Ref. [18]. Another example is terms involving the coefficients $c_{L,R,Q,U,D}$, some of which can be absorbed via field normalization redefinition. The Lorentz violating Yukawa terms are studied in the following section.

1.5 Lorentz violating Yukawa sector: renormalizable extension

Because the mSME is an effective field theory that parametrizes heavy physics at SM energy scales, its Lagrangian terms are solely defined in terms of the fields of such a low energy description. Lorentz non conserving interactions are introduced in all SM sectors in this context, among which we consider Lagrangian terms from the Yukawa sector for the phenomenological objectives of the present investigation. For the time being, $SU(3)_C \times SU(2)_L \times U_Y(1)$ gauge symmetry is assumed and then spontaneously broken using the Brout-Englert-Higgs mechanism [94–96] as usual, in order to define the full set of mass eigenfields within the theory governed by the electromagnetic gauge group [97–101]. This procedure has an impact on Lorentz violating interactions, which calls for a discussion of the resulting terms of the mSME Yukawa sector.

The renormalizable version of the SME is given by

$$\mathcal{L}_{\text{R}}^{\text{SME}} = \mathcal{L}^{\text{SM}} + \Delta\mathcal{L}^{\text{R}}, \tag{1.9}$$

where $\mathcal{L}^{\text{SM}}$ denotes the SM Lagrangian. $\Delta\mathcal{L}^{\text{R}}$, containing all power counting renormalizable interactions, is the sum of the terms with the form $\mathcal{T}^{\mu_1,\ldots,\mu_n}\mathcal{O}_{\mu_1,\ldots,\mu_n}(x)$, where $\mathcal{O}_{\mu_1,\ldots,\mu_n}(x)$ represents $SU(3)_C \times SU(2)_L \times U_Y(1)$ invariant operators of the SME, and $\mathcal{T}^{\mu_1,\ldots,\mu_n}$ are constant background fields.

This section focuses on the CPT even renormalizable extension of the leptonic Yukawa sector that induces lepton flavor violation (LFV) via the Higgs boson, given by [7]

$$\begin{aligned}
\mathcal{L}_{\text{Yukawa}}^{\text{SME}} = &- (Y_L)^{AB}\bar{L}_A\phi R_B - \frac{1}{2}(H_L)_{\mu\nu}^{AB}\bar{L}_A\phi\sigma^{\mu\nu}R_B \\
&- (Y_U)^{AB}\bar{Q}_A\phi^c U_B - \frac{1}{2}(H_U)_{\mu\nu}^{AB}\bar{Q}_A\phi^c\sigma^{\mu\nu}U_B \\
&- (Y_D)^{AB}\bar{Q}_A\phi D_B - \frac{1}{2}(H_D)_{\mu\nu}^{AB}\bar{Q}_A\phi\sigma^{\mu\nu}D_B + \text{h.c.}\,,
\end{aligned} \tag{1.10}$$

where ϕ is the Higgs doublet with its conjugate ϕ^c. $(Y_L)^{AB}, (Y_U)^{AB}$ and $(Y_D)^{AB}$ are the SM Yukawa matrices, which are complex valued matrices in general and not necessarily symmetric or Hermitian. L_A and R_A are the SM $SU(2)_L$ left handed lepton doublet and right handed lepton singlet respectively. Q_A is the right handed quark doublet, whereas U_A and D_A are the u and d type right handed quark singlets. A, B label the fermion flavor and greek indices label the spacetime components. The dimensionless matrices with entries $(H_L)_{\mu\nu}^{AB}$, $(H_U)_{\mu\nu}^{AB}$ and $(H_D)_{\mu\nu}^{AB}$ are antisymmetric in the Lorentz indices but symmetric, although not necessarily Hermitian, in flavor space. According to Eq. (1.9), the left half of $\mathcal{L}_{\text{Yukawa}}^{\text{SME}}$ corresponds to SM terms, while the right half corresponds to Lorentz violating terms. These last terms open up the possibility of flavor violation effects mediated by the Higgs bosson. In what follows, we will only focus on the lepton sector; however, we can mention that in the quark sector, we analyze the EMMs of neutron and proton [102].

Let's analyze the spontaneous symmetry breaking. Changing the variable in unitary gauge to the Higgs doublet, $\phi = \phi_0 + h$, with $\phi_0 = \left(\begin{smallmatrix}0\\v/\sqrt{2}\end{smallmatrix}\right)$, and using it in Eq. (1.10), we get

$$\mathcal{L}_{\text{Yukawa}}^{\text{SME}} = -\frac{1}{\sqrt{2}}(v + H)\left(\vec{\bar{l}}'_L\, Y'_l\, \vec{l}'_R + \frac{1}{2}\vec{\bar{l}}'_L\,(H_l)_{\mu\nu}\,\sigma^{\mu\nu}\,\vec{l}'_R + \text{h.c.}\right)\,, \tag{1.11}$$

where $\vec{l}' = (e', \mu', \tau')$ is a vector in flavor space. Performing the change of bases from $(\vec{l}'_L, \vec{l}'_R)$ to the mass eigenstate basis $(\vec{l}_L, \vec{l}_R)$ via unitary transformations

$$\begin{aligned}
\vec{l}'_L &= V_L^\dagger\, \vec{l}_L, \\
\vec{l}'_R &= V_R^\dagger\, \vec{l}_R,
\end{aligned} \tag{1.12}$$

where $V_{L,R}$ are the standard unitary matrices that connect the gauge and mass eigenfields bases of chiral spinors. This transformation, as well known, diagonalize, at the same time, the mass terms and Higgs lepton interactions in the SM, however, in this case, the Lorentz violating extension introduces non diagonal couplings.

$$\mathcal{L}_{\text{Yukawa}}^{\text{SME}} = -\sum_A \left(m_{l_A} + \frac{g m_{l_A}}{2 m_w} H \right) \bar{l}_A\, l_A - \frac{1}{2} \sum_{AB} (v+H)\, \bar{l}_A \left(\frac{Y_{\mu\nu}^{AB} + Y_{\mu\nu}^{BA*}}{2} + \frac{Y_{\mu\nu}^{AB} - Y_{\mu\nu}^{BA*}}{2} \gamma^5 \right) \sigma^{\mu\nu} l_B.$$

(1.13)

In the above expression $Y_{\mu\nu} = V_L^\dagger H_{\mu\nu} V_R$. Despite the fact that the notation of matrices $Y_{\mu\nu}$ does not explicitly indicate it, three types of fermions correspond to each of them, namely, $Y_{\mu\nu}^L$, $Y_{\mu\nu}^D$, and $Y_{\mu\nu}^U$, which stand for charged leptons, u type quarks, and d type quarks, respectively.

Defining

$$V_{\mu\nu}^{AB} = \frac{Y_{\mu\nu}^{AB} + Y_{\mu\nu}^{BA*}}{2},$$
$$A_{\mu\nu}^{AB} = \frac{Y_{\mu\nu}^{AB} - Y_{\mu\nu}^{BA*}}{2},$$

(1.14)

we get, from Eq. (1.13), the following expression

$$\mathcal{L}_{\text{Yukawa}}^{\text{SME}} = -\sum_A \left(m_{l_A} + \frac{g m_{l_A}}{2 m_w} H \right) \bar{l}_A\, l_A - \frac{1}{2} \sum_{AB} (v+H)\, \bar{l}_A \left(V_{\mu\nu}^{AB} - A_{\mu\nu}^{BA*} \gamma^5 \right) \sigma^{\mu\nu} l_B. \qquad (1.15)$$

The aim of the previous process was to pass from the gauge basis to the mass eigenstates basis.

According to the definition of $V_{\mu\nu}^{AB}$ and $A_{\mu\nu}^{AB}$, note from Eq. (1.14) that the matrix $V_{\mu\nu}$ is Hermitian, whereas matrix $A_{\mu\nu}$ is antihermitian with respect to flavor space. Note, from Eq. (1.14) that $A_{\mu\nu}$ vanishes for Hermitian matrix Y, that is, if $Y_{\mu\nu}^\dagger = Y_{\mu\nu}$, whereas the antiHermitian matrix condition $Y_{\mu\nu}^\dagger = -Y_{\mu\nu}$, eliminates $V_{\alpha\beta}$. On the other hand, matrices V^{AB} and A^{AB}, given in spacetime group, are both antisymmetric, $V_{\mu\nu}^{AB} = -V_{\nu\mu}^{AB}$ and $A_{\mu\nu}^{AB} = -A_{\nu\mu}^{AB}$, this is inherited from the antisymmetric property of the Y^{AB} matrix.

In the perturbative approach, used here, the Lorentz violating Yukawa couplings, from Eq.(1.15) produce two types of physical couplings:

$$\text{bililear insertion:} \quad -\frac{v}{2} \bar{l}_A (V_{\mu\nu}^{AB} - A_{\mu\nu}^{BA*} \gamma^5) \sigma^{\mu\nu} l_B \,,$$
$$\text{trilinear vertex:} \quad -\frac{1}{2} H \bar{l}_A (V_{\mu\nu}^{AB} - A_{\mu\nu}^{BA*} \gamma^5) \sigma^{\mu\nu} l_B \,,$$

which leads to the bilinear coupling, with the vertex

$$\underset{l_A}{\rule{0pt}{0pt}} \;\bullet\; \underset{l_B}{\rule{0pt}{0pt}} \qquad = \quad \frac{-iv}{2}(V_{\mu\nu}^{AB} - A_{\mu\nu}^{BA\,*}\gamma^5)\sigma^{\mu\nu} \; ,$$

and contains the LFV coupling of the Higgs boson $Hl_A l_B$, whose vertex function is given by

$$-\,-\,\overset{H}{-}\,-\,\bullet\!\!<\begin{array}{l}l_A\\[1em]l_B\end{array} \qquad = \quad \frac{-i}{2}(V_{\mu\nu}^{AB} - A_{\mu\nu}^{BA\,*}\gamma^5)\sigma^{\mu\nu} \; .$$

Chapter 2

One loop contributions to lepton electromagnetic interactions

Under the assumption of Lorentz invariance, contributions to AMMs and EDMs are obtained from the electromagnetic vertex parametrization $A_\mu l_A l_A$ given by $\bar{u}_A(p')\Gamma_\mu u_A(p)$ with u_A the momentum space Dirac spinors for the charge lepton l_A with mass m_A and Γ_μ being [103–105]

$$\Gamma_\mu = ie\left[\gamma^\mu(f_V^A - f_A^A \gamma_5) - \sigma_{\mu\nu}q^\nu\left(i\frac{f_m^A}{2m_A} - \frac{f_d^A}{e}\gamma_5\right)\right], \tag{2.1}$$

with on shell external fermions and off shell photon field. $f_{V,A,m,d}^A$ are the charge, anapole, magnetic and electric dipole lepton form factors respectively. In general, all the form factors are functions of squared transferred photon momentum q^2 and lepton masses. The on shell photon case ($q^2 = 0$) defines the AMM and EDM by $a^A \equiv \frac{2m_A}{e}f_m^A(q^2 = 0)$ and $d^A \equiv f_d^A(q^2 = 0)$, respectively. Those terms are necessarily originated at second order SME coefficient contributions because, in this way, all the Lorentz indexes are fully contracted.

We calculate the contributions, at one loop, to the electromagnetic vertex $A_\mu l_A l_A$ from the Lorentz violation Yukawa sector $\mathcal{L}_{\text{Yukawa}}^{\text{SME}}$, as shown in Eq. (1.15). The sectors of the lepton and the Higgs boson produce couplings in the minimal SME CPT, which can also produce contributions to lepton electromagnetic moments. In the case of the lepton Lagrangian terms, Eq. (1.8a), such contributions would come from the antisymmetric parts of SME coefficients $c_{\mu\nu}$, which can be removed from the theory by redefining spinor fields appropriately [106]. The contributions from the aforementioned Lorentz violating Higgs sector, on the other hand, have a suppressing factor $\frac{1}{m_w^4}$ in comparison to the contributions calculated in the present investigation, so we ignore them. Finally, keep in mind that, as part of an effective field theory, the SME Lagrangian terms may not all be produced by the genuine fundamental physical description.

It is critical to note that the contributions to the general electromagnetic vertex $A_\mu l_A l_B$ are taken into account, with l_A and l_B being equal. As explicitly demonstrated in Refs. [33, 34], the occurrence

of Lorentz symmetry violation modifies electromagnetic interactions at the loop level, and the structure of this interaction parametrization is expected to be richer with more types of terms than those in Eq. (1.15), due to all free spacetime indexes, but AMMs and EDMs are still identified from the aforementioned Lorentz preserving parametrization [103–105], which means that Lorentz violating background fields can only be contracted with themselves. According to Eq. (1.14), because coefficients $V_{\mu\nu}^{AB}$ and $A_{\mu\nu}^{AB}$ are antisymmetric in terms of spacetime indices, they are traceless in this sense. Consequently, any first order contribution to AMMs and EDMs vanishes. However, nonzero Lorentz invariant contributions may appear if diagrams at the second order in $V_{\mu\nu}^{AB}$ or $A_{\mu\nu}^{AB}$ are considered.

2.1 Contribution from Feynman diagrams

The contribution to the electromagnetic moment of the leptons l_A, with $A = e, \mu, \tau$, defined in Eq. (2.1), is produced by the sum of all Feynman diagrams in which either two point insertion appear, Fig. (2.1), or two three point vertices or simultaneously one two point insertion and one three point vertex appear, Fig. (2.2). Furthermore, we can see that the entire set of contributing diagrams consists of diagrams with virtual lines for the Z boson, photon, and Higgs boson. These particles are depicted with a double line inside the loop in Fig. (2.1), whereas the Higg boson virtual particle is the only possibility in Fig. (2.2) due to the interactions depicted in Eq. (1.15). Because neutrinos are considered to be massless, no couplings between them and the Higgs field occur, resulting in the absence of contributing diagrams with virtual W boson lines.
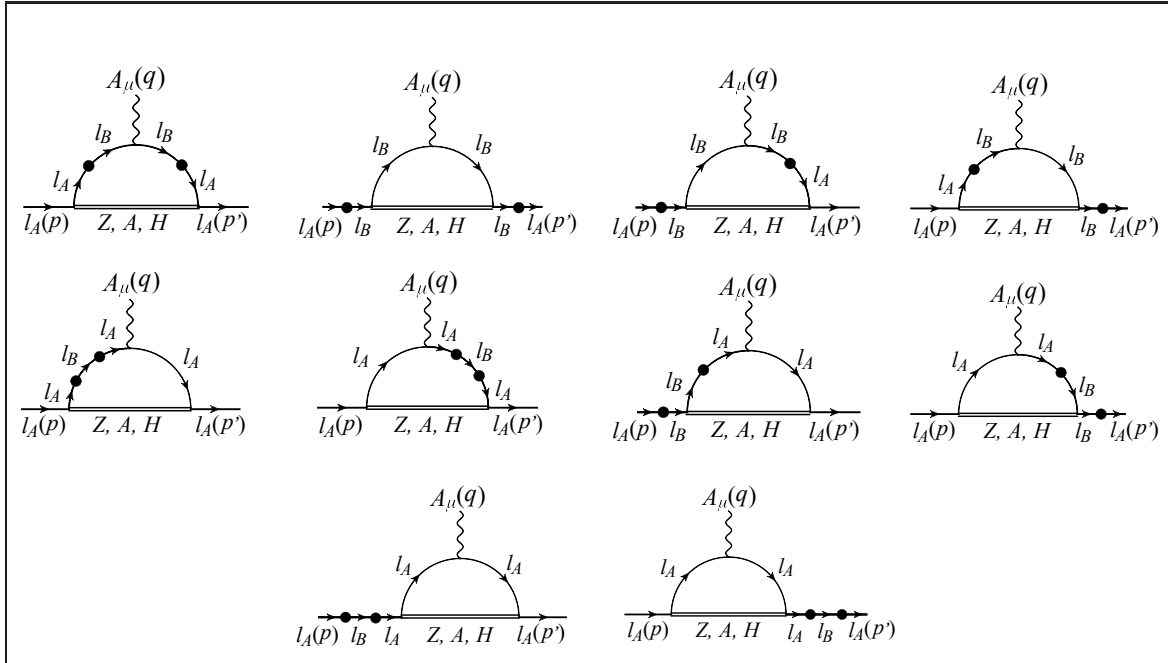

Figure 2.1: Feynman diagrams $A_\mu l_A l_A$ that contribute to magnetic and electric form factors, Lorentz-noconservation effects enter only through bilinear insertions $l_A l_B$, where $A = B$ or $A \neq B$. Z boson, photon, or Higgs boson are represented by virtual double lines in loops.

It is important noting that both two point insertions and three point vertices generated by Eq.
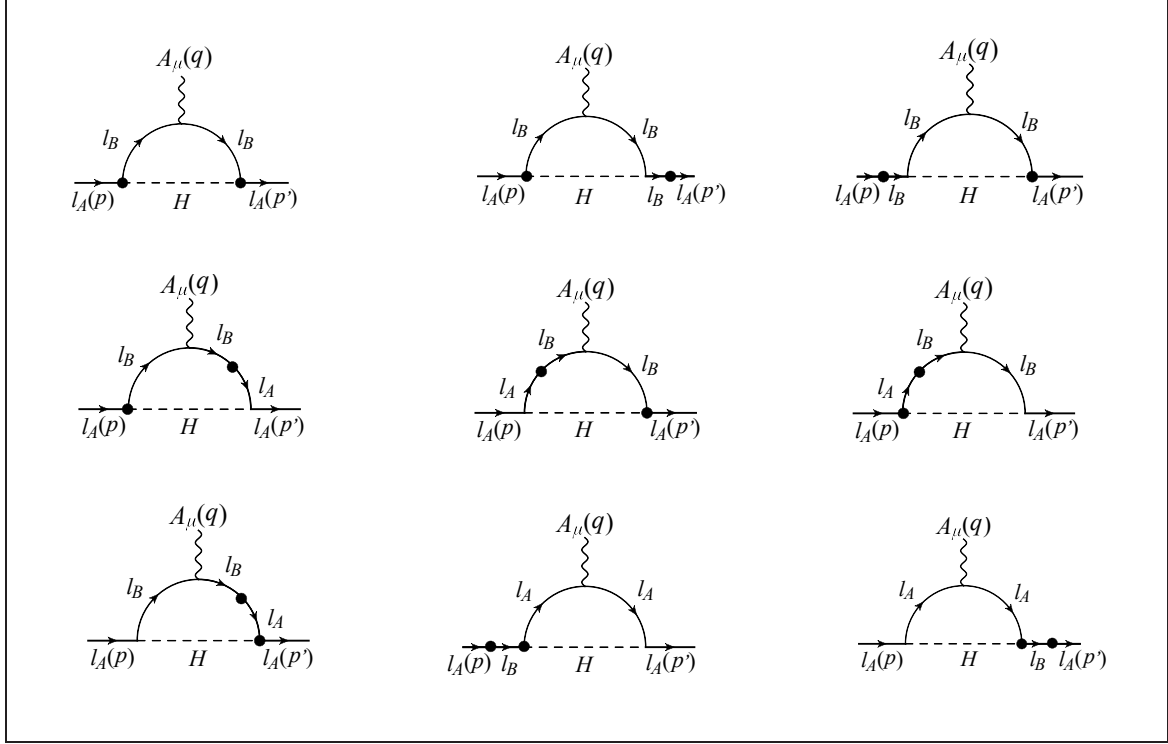
Figure 2.2: Feynman diagrams $A_\mu l_A l_A$ contributing to magnetic and electric form factors, with Lorentz non conservation effects entering through both bilinear insertions $l_A l_B$ and three point vertices $H l_A l_B$, where either $A = B$ or $A \neq B$. In order to exist, these diagrams must contain a virtual Higgs boson line.

(1.15) are flavor changing, which enlarges the number of contributing diagrams. However, it is worth emphasizing that the initial and final particle flavors are always the same. We perform this calculation in the unitary gauge. As a result, there are no diagrams with pseudo Goldstone bosons.

If we look closely at each diagram in Figs. (2.1) and (2.2), we can divide them into two groups:

1. Diagrams with lepton flavor change, inside the loop, due to the presence of anomalies, that is $A \neq B$, which we call *virtual lepton flavor change.*

2. Diagrams in which there is no lepton flavor change due to the presence of the insertions, i.e. $A = B$, which we refer to as *virtual lepton flavor conservation.*

All calculations were carried out using the (Passarino Veltman) PaVe tensor reduction method [107], for which we used the Wolfram software Mathematica, as well as the packages FeynCalc [108] and Package-X [109]. The presence of two point insertions in contributing Feynman diagrams introduces technical complexities. The Lorentz violating coefficients broaden the set of Lorentz structures involved in the loop contributions to AMMs and EDMs. The generated form factor expressions are also quite large. Another practical complication arises from the fact that each bilinear insertion introduces an extra loop denominator, so loop integrals involve multiple propagator denominators, for which calculation strategies were developed and implemented.

2.2   Dominant contributions to AMM and EDM

Two significant considerations must be made in order to calculate the electromagnetic vertex $A_\mu l_A l_A$. (1) Because virtual photon diagrams, shown in Fig. 2.1, are associated with infrared divergences (IR), we propose a fictitious virtual photon mass, m_γ [97–101]. This method will be emphasized in the following paragraphs. (2) We take both external fermions on shell and keep the external photon field off shell, that is $q^2 \neq 0$, only scalar PaVe functions can be obtained as a result of this.

With the preceding information in mind, all electromagnetic form factors are intricate functions of the lepton mass, m_A, and q^2. As well as functions of Higgs boson, m_H, Z boson, m_Z and the fictitious virtual photon m_γ masses, according to the corresponding diagram calculated from Figs. (2.1- 2.2).

The diagrams with virtual photon inside the loop make the most significant contributions to the EDMs and AMMs (see Fig. 1). In general, the photon propagator introduces a factor $1/k^2$ (without accounting for the fictitious mass), where k is the four momentum that will be integrated. However, the propagators of the Z and Higgs bosons are $1/(k^2 - m_{Z,H}^2)$. The suppression of the Z and Higgs boson contributions occurs later in the integration of the four momentum because it produces powers of the factor $1/m_{Z,H}$ and photon does not, enhancing its contribution. The difference in quantitative terms between such dominant contributions and those resulting from other diagrams is at least ten orders of magnitude. While all diagrams have been calculated and their contributions estimated, we will only focus on the contributions due to the virtual photon propagator diagrams and ignore all other contributions in the following.

We only consider the three diagrams in Fig. 2.3 for the virtual photon line. These diagrams have been identified as producing the leading contributions among the entire set of virtual photon diagrams, and have Lorentz violating two point insertions in loop lines exclusively.
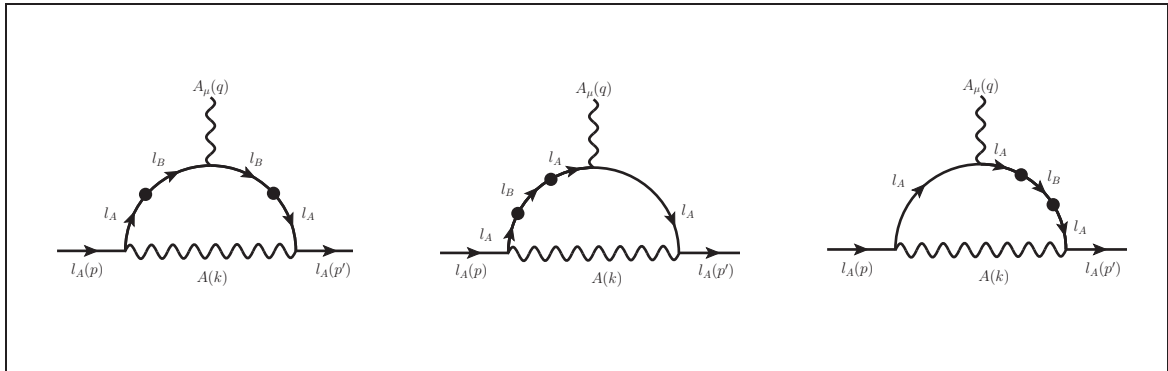
Figure 2.3: Feynman diagrams $A_\mu l_A l_A$ that produce the leading contribution.

Analytic expressions of triangle diagrams, written in the unitary gauge, have three propagator denominators and are applicable to a wide range of models. However, using two point insertions in this calculation produces expressions with up to five such denominators, which makes the analytic calculation more difficult. To calculate the loop integrals, we use two methods: i) Using squared-mass derivatives,

the number of propagator denominators, in loop integrals, is reduced to three. ii) The procedure, which includes all propagators, requires the direct computation of four and five point PaVe scalar functions [107]. We verified that the results obtained by both strategies are identical.

2.2.1 Squared-mass derivatives procedure

We write the analytical expression of the first diagram (from left to right) of Fig. 2.3 using the Feynman parametrization technique [97] as shown below

$$
\begin{aligned}
\Gamma_{1\mu}^{AB} &= \frac{i}{(4\pi)^2} \frac{(2\pi\mu)^{4-D}}{i\pi} \int d^D k \frac{N_{1\mu}(m_A, m_B)}{[(k+p)^2 - m_A^2][(k+p)^2 - m_B^2][(k+p')^2 - m_B^2][(k+p')^2 - m_A^2][k^2 - m_\gamma^2]} \\
&= \frac{i}{(4\pi)^2} \frac{(2\pi\mu)^{4-D}}{i\pi} \int d^D k \frac{N_{1\mu}(m_A, m_B)}{\Delta_A(p)\,\Delta_B(p)\,\Delta_B(p')\,\Delta_A(p')\,\Delta_\gamma},
\end{aligned} \tag{2.2}
$$

where $\Delta_\gamma = k^2 - m_\gamma^2$ and $\Delta_j(p) = (k+p)^2 - m_j^2$. The mass of the initial and final lepton states is m_A, and m_B corresponds to the mass of the lepton inside the loop. The indices $A,B = e, \mu, \tau$.

The following expression applies to the numerator $N_{1\mu}(m_A, m_B)$

$$
\begin{aligned}
N_{1\mu}(m_A, m_B) = -\frac{e^3 v^2}{4} \gamma^\nu (\slashed{k} + \slashed{p}' + m_A)(V_{\alpha\beta}^{AB} + A_{\alpha\beta}^{BA*}\gamma_5)\sigma^{\alpha\beta}(\slashed{k} + \slashed{p}' + m_B) \\
\times \gamma_\mu (\slashed{k} + \slashed{p} + m_B)(V_{\rho\lambda}^{AB} + A_{\rho\lambda}^{BA*}\gamma_5)\sigma^{\rho\lambda}(\slashed{k} + \slashed{p} + m_A)\gamma_\nu \,.
\end{aligned} \tag{2.3}
$$

Making use of the identity [97]

$$
\frac{1}{\Delta_A(p)\Delta_A(p')} = \int_0^1 dx \frac{1}{[x\Delta_A(p) + (1-x)\Delta_A(p')]^2}, \tag{2.4}
$$

as well as employing kinematical conditions for external leptons, $p^2 = p'^2 = p \cdot p' = m_A^2$, we get

$$
\frac{1}{\Delta_A(p)\Delta_A(p')} = \int_0^1 dx \frac{1}{[(k+l)^2 - m_A^2]^2} = \frac{\partial}{\partial m_j^2} \int_0^1 dx \frac{1}{\Delta_j(l)}\bigg|_{m_j^2 = m_A^2} \tag{2.5}
$$

where $l = xp + (1-x)p'$. In this fashion, we can use twice Eq. 2.5 in the expression 2.2 to obtain a shorter result

$$
\Gamma_{1\mu}^{AB} = \frac{i}{(4\pi)^2} \frac{(2\pi\mu)^{4-D}}{i\pi} \int d^D k \int_0^1 \int_0^1 dx\, dy \frac{\partial}{\partial m_j^2} \frac{\partial}{\partial m_k^2} \frac{N_{1\mu}(m_A, m_B)}{\Delta_j(l)\Delta_k(l')\Delta_\gamma}\bigg|_{\substack{m_j^2 = m_A^2 \\ m_k^2 = m_B^2}}, \tag{2.6}
$$

in which $l' = yp + (1-y)p'$ and l was defined previously.

The expression for the middle diagram in Fig. 2.3 is

$$\Gamma_{2\mu}^{AB} = \frac{i}{(4\pi)^2}\frac{(2\pi\mu)^{4-D}}{i\pi}\int d^D k \frac{N_{2\mu}(m_A, m_B)}{[(k+p)^2 - m_A^2]^2[(k+p)^2 - m_B^2][(k+p')^2 - m_A^2][k^2 - m_\gamma^2]}$$

$$= \frac{i}{(4\pi)^2}\frac{(2\pi\mu)^{4-D}}{i\pi}\int d^D k \frac{N_{2\mu}(m_A, m_B)}{\Delta_A^2(p)\,\Delta_B(p)\,\Delta_A(p')\,\Delta_\gamma}, \tag{2.7}$$

where

$$N_{2\mu} = -\frac{e^3 v^2}{4}\gamma^\nu(\slashed{k} + \slashed{p}' + m_A)\gamma_\mu(\slashed{k} + \slashed{p} + m_A)(V_{\alpha\beta}^{AB} + A_{\alpha\beta}^{BA\,*}\gamma_5)\sigma^{\alpha\beta}$$

$$\times (\slashed{k} + \slashed{p} + m_B)(V_{\rho\lambda}^{AB} + A_{\rho\lambda}^{BA\,*}\gamma_5)\sigma^{\rho\lambda}(\slashed{k} + \slashed{p} + m_A)\gamma_\nu. \tag{2.8}$$

For this case, it is convenient to apply the derivative with respect to $\Delta_A(p)$ on both sides of the equation 2.4

$$\frac{-1}{\Delta_A^2(p)\Delta_A(p')} = (-2)\int_0^1 \frac{x}{[x\Delta_A(p) + (1-x)\Delta_A(p')]^3}, \tag{2.9}$$

adding the same kinematical conditions mentioned previously for the denominator expression yields

$$\frac{1}{\Delta_A^2(p)\Delta_A(p')} = 2\int_0^1 dx \frac{x}{[(k+l)^2 - m_A^2]^3} = \frac{\partial^2}{\partial(m_j^2)^2}\int_0^1 dx \frac{x}{\Delta_j(l)}\bigg|_{m_j^2 = m_A^2}. \tag{2.10}$$

If we use Eq. 2.10 in Eq. 2.7, we reduce the number of denominators

$$\Gamma_{2\mu}^{AB} = \frac{i}{(4\pi)^2}\frac{(2\pi\mu)^{4-D}}{i\pi}\int d^D k \int_0^1 dx \frac{\partial^2}{\partial(m_j^2)^2}\frac{x\,N_{2\mu}(m_A, m_B)}{\Delta_j(l)\Delta_B(p)\Delta_\gamma}\bigg|_{m_j^2 = m_A^2}. \tag{2.11}$$

The third diagram (from left to right) in Fig. 2.3

$$\Gamma_{3\mu}^{AB} = \frac{i}{(4\pi)^2}\frac{(2\pi\mu)^{4-D}}{i\pi}\int d^D k \frac{N_{3\mu}(m_A, m_B)}{[(k+p')^2 - m_A^2]^2[(k+p')^2 - m_B^2][(k+p)^2 - m_A^2][k^2 - m_\gamma^2]}$$

$$= \frac{i}{(4\pi)^2}\frac{(2\pi\mu)^{4-D}}{i\pi}\int d^D k \frac{N_{3\mu}(m_A, m_B)}{\Delta_A^2(p')\,\Delta_B(p')\,\Delta_A(p)\,\Delta_\gamma}, \tag{2.12}$$

requires a similar procedure to the previous one. The difference is that we must derive both sides of Eq. 2.4 with respect to $\Delta_A(p')$ and apply in the diagram expression, resulting in

$$\Gamma_{3\mu}^{AB} = \frac{i}{(4\pi)^2}\frac{(2\pi\mu)^{4-D}}{i\pi}\int d^D k \int_0^1 dx \frac{\partial^2}{\partial(m_j^2)^2}\frac{(1-x)\,N_{3\mu}(m_A, m_B)}{\Delta_j(l)\Delta_B(p')\Delta_\gamma}\bigg|_{m_j^2 = m_A^2}, \tag{2.13}$$

the expression for the numerator $N_{3,\mu}(m_A, m_B)$ is

$$N_{3\mu} = -\frac{e^3 v^2}{4}\gamma^\nu(\slashed{k} + \slashed{p}' + m_A)(V_{\alpha\beta}^{AB} + A_{\alpha\beta}^{BA\,*}\gamma_5)\sigma^{\alpha\beta}(\slashed{k} + \slashed{p}' + m_B)$$

$$\times (V_{\rho\lambda}^{AB} + A_{\rho\lambda}^{BA\,*}\gamma_5)\sigma^{\rho\lambda}(\slashed{k} + \slashed{p}' + m_A)\gamma_\mu(\slashed{k} + \slashed{p} + m_A)\gamma_\nu. \tag{2.14}$$

The total contribution is

$$\Gamma_\mu^A = \sum_{B=e,\mu\tau} (\Gamma_{1\mu}^{AB} + \Gamma_{2\mu}^{AB} + \Gamma_{3\mu}^{AB}). \tag{2.15}$$

Equations (2.6) - (2.13) cover all cases in which virtual lepton flavor is conserved and changed within the loop. In these equations, loop integrals are regularized using the dimensional regularization approach [97, 110], where μ is a quantity, with units of mass, introduced to correct amplitude mass dimensions. The factors $N_{j\mu} = N_{j\mu}(m_A, m_B)$, shown in Eqs. (2.3), (2.8) and (2.14), depending on the charged lepton masses, are unaffected by squared mass derivatives.

The other method, which includes all propagators, requires evaluating all of the integrals shown in the first parts of Eqs. (2.2 - 2.12). As previously stated, we obtain the same results as the derivatives method; however, carrying all five propagator denominators increases the time required for calculation.

2.3 Electromagnetic form factors

Solving the corresponding loop integrals, using the Gordon identities and carrying out algebraic manipulations, we write the total contributions as

$$\Gamma_\mu^A = \frac{e}{2m_A} f_m^A \sigma_{\mu\nu} q^\nu + i f_d^A \sigma_{\mu\nu} q^\mu \gamma_5 + ..., \tag{2.16}$$

where f_m^A and f_d^A are the magnetic and electric forms factors, respectively which depend on field masses, squared photon momentum q^2, and quadratic products of Lorentz tensor coefficients $V_{\alpha\beta}^{AB}$ and $A_{\alpha\beta}^{BA*}$.

f_A^m and f_A^d, from Eq. (2.1), are invariant under particle Lorentz transformations. As a result, contributions to the AMM and EDM of the charged lepton l_A can be easily extracted from such coefficients. That is, we will only consider terms that are invariant under Lorentz symmetry transformations and proportional to $\sigma_{\mu\nu} q^\nu$ and $\sigma_{\mu\nu} q^\nu \gamma_5$. In this way, the ellipsis in Eq. (2.16) represents the large set of terms that involve violations of invariance under particle Lorentz transformations. These terms are proportional to the components of the four momenta; p^α, p^β, p^ρ and p^λ, and the same with p', We do not take them into account because they are dependent on the reference system and are not part of AMM and EDM.

The magnetic form factor is a function of the squared products $V_{\alpha\nu}^{AB}V^{AB\nu\beta}$, $A_{\alpha\nu}^{BA*}A^{BA\nu\beta*}$, and the electric form factor a is function of $V_{\alpha\nu}^{AB}A^{BA\nu\beta*}$. For convenience, we define the 4×4 matrix with entries

$$(\kappa_1^{AB})_\alpha^{\ \beta} = V_{\alpha\nu}^{AB}V^{AB\nu\beta}, \tag{2.17}$$

$$(\kappa_2^{AB})_\alpha^{\ \beta} = A_{\alpha\nu}^{BA*}A^{BA\nu\beta*}, \tag{2.18}$$

$$(\kappa_3^{AB})_\alpha^{\ \beta} = V_{\alpha\nu}^{AB}A^{BA\nu\beta*}. \tag{2.19}$$

Counting the different complex matrices κ_1^{AB}, we have: 1) κ_1^{ee}, 2) $\kappa_1^{e\mu}$, 3)$\kappa_1^{e\tau}$, 4)$\kappa_1^{\mu e}$, 5)$\kappa_1^{\mu\mu}$, 6)$\kappa_1^{\mu\tau}$, 7)$\kappa_1^{\tau e}$, 8)$\kappa_1^{\tau\mu}$ and 9)$\kappa_1^{\tau\tau}$, the same for κ_2^{AB} and κ_3^{AB}. There are 27 of the matrices. Because their entries are complex, each matrix with spacetime indices has 32 parameters, for a total of 864 parameters. These parameters are not independent because the kappa matrices have some properties that follow from the V^{AB} and A^{AB} definition, shown in Eq. (1.14)

$$(\kappa_1^{AB})_\alpha{}^\beta = V_{\alpha\nu}^{AB}V^{AB\nu\beta} = (-V_{\beta\nu}^{AB})(-V^{AB\nu\alpha}) = (\kappa_1^{AB})_\beta{}^\alpha, \tag{2.20}$$

$$(\kappa_2^{AB})_\alpha{}^\beta = A_{\alpha\nu}^{BA*}A^{BA\nu\beta*} = (-A_{\beta\nu}^{BA*})(-A^{BA\nu\alpha*}) = (\kappa_2^{AB})_\beta{}^\alpha, \tag{2.21}$$

$$(\kappa_1^{AB})_\alpha{}^\beta = V_{\alpha\nu}^{AB}V^{AB\nu\beta} = V_{\alpha\nu}^{BA*}V^{BA\nu\beta*} = (\kappa_1^{BA*})_\alpha{}^\beta, \tag{2.22}$$

$$(\kappa_2^{AB})_\alpha{}^\beta = A_{\alpha\nu}^{BA*}A^{BA\nu\beta*} = (-A_{\alpha\nu}^{AB})(-A^{AB\nu\beta}) = (\kappa_2^{BA*})_\alpha{}^\beta, \tag{2.23}$$

$$(\kappa_3^{AB})_\alpha{}^\beta = V_{\alpha\nu}^{AB}A^{BA\nu\beta*} = V_{\alpha\nu}^{BA*}(-A^{AB\nu\beta}) = -(\kappa_3^{BA*})_\alpha{}^\beta. \tag{2.24}$$

We can deduce from Eqs. (2.22) and (2.23) that $(\kappa_j^{AB})_{\alpha\beta} = \mathrm{Re}(\kappa_j^{AB})$, for $j = 1, 2$ and $(\kappa_3^{AB})_{\alpha\beta} = i\,\mathrm{Im}(\kappa_3^{AB})$. Because of the spacetime indices, the entire set of matrices consists of 27 elements, each with 16 real entries. Using cases (2.20) and (2.21), however, a further reduction occurs due to symmetry in the space of matrix Lorentz representation for κ_j, where $j = 1, 2$, resulting in a matrix with 10 real entries. After these considerations, the number of parameters resulting from complex quantities are

Parameters	$(\kappa_1^{AB})_\alpha{}^\beta$	$(\kappa_2^{AB})_\alpha{}^\beta$	$(\kappa_3^{AB})_\alpha{}^\beta$
Number	$9 \times 10 = 90$	$9 \times 10 = 90$	$9 \times 16 = 144$

resulting 324 parameters. In this case, however, the Lorentz violating contributions to AMMs and EDMs do not contain information on all these parameters. We will demonstrate below that all Lorentz violating contributions from the Yukawa sector to AMM and EDM emerge as linear combinations of traces $\mathrm{tr}\kappa_j^{AB} = (\kappa_j^{AB})_\alpha{}^\alpha$, which are the quantities to be bound.

The total contribution for the l_A lepton magnetic and electric form factors, f_m^A and f_d^A respectively, come from the sum over those diagrams with virtual lepton flavor conserving, $f_{m,d}^{AA}$, and those with virtual lepton flavor change $f_{m,d}^{AB}$, with $A \neq B$. That is

$$f_m^A = f_m^{AA} + \sum_{B \neq A} f_m^{AB}, \tag{2.25}$$

$$f_d^A = f_d^{AA} + \sum_{B \neq A} f_d^{AB}. \tag{2.26}$$

Every contribution to the electromagnetic form factors is a function of the Lorentz violating coefficients squared product

$$f_m^{AA} = h_{m,1}^{AA} V_{\alpha\nu}^{AA} V^{AA\nu\alpha} + h_{m,2}^{AA} A_{\alpha\nu}^{AA\,*} A^{AA\nu\alpha*}, \tag{2.27}$$

$$f_d^{AA} = h_{d,3}^{AA} V_{\alpha\nu}^{AA} A^{AA\nu\alpha*}, \tag{2.28}$$

$$f_m^{AB} = h_{m,1}^{AB} V_{\alpha\nu}^{AB} V^{AB\nu\alpha} + h_{m,2}^{AB} A_{\alpha\nu}^{BA\,*} A^{BA\nu\alpha*}, \tag{2.29}$$

$$f_d^{AB} = h_{d,3}^{AB} V_{\alpha\nu}^{AB} A^{BA\nu\alpha*}, \tag{2.30}$$

where all the h^{AA}, Eqs. (2.27) and (2.28), are functions of m_A, q^2, m_γ, x, y. For these functions we will use the mass derivatives method. The other scalar functions h^{AB}, given in Eqs. (2.29) and (2.30), are functions of m_A, m_B. For these functions we will use four and five point PaVe Functions. Due to the invariance of electromagnetic form factors under Lorentz transformations, all Lorentz indices must be contracted in the squared products of A^{AB} and V^{AB}.

According to the definitions shown in (2.17)-(2.19), observe the following

$$V_{\alpha\nu}^{AB} V^{AB\nu\alpha} = (\kappa_1^{AB})_\alpha{}^\alpha = \mathrm{tr}\kappa_1^{AB}, \tag{2.31}$$

$$A_{\alpha\nu}^{BA\,*} A^{BA\nu\alpha*} = (\kappa_2^{AB})_\alpha{}^\alpha = \mathrm{tr}\kappa_2^{AB}, \tag{2.32}$$

$$V_{\alpha\nu}^{AB} A^{BA\nu\alpha*} = (\kappa_3^{AB})_\alpha{}^\alpha = \mathrm{tr}\kappa_3^{AB}. \tag{2.33}$$

That is to say, all of the form factors are functions of the traces $\mathrm{tr}\kappa_j$ with $j = 1, 2, 3$. The magnetic form factor is expressed in terms of $\mathrm{tr}\kappa_1$ and $\mathrm{tr}\kappa_2$, whereas the electric form factor is expressed only in terms of $\mathrm{tr}\kappa_3$.

$$f_m^{AA} = h_{m,1}^{AA} \mathrm{tr}\kappa_1^{AA} + h_{m,2}^{AA} \mathrm{tr}\kappa_2^{AA}, \tag{2.34}$$

$$f_d^{AA} = h_{d,3}^{AA} \mathrm{tr}\kappa_3^{AA}, \tag{2.35}$$

$$f_m^{AB} = h_{m,1}^{AB} \mathrm{tr}\kappa_1^{AB} + h_{m,2}^{AB} \mathrm{tr}\kappa_2^{BA\,*}, \tag{2.36}$$

$$f_d^{AB} = h_{d,3}^{AB} \mathrm{tr}\kappa_3^{AB}, \tag{2.37}$$

where the symbol "tr" denotes, as before, a trace operating on 4×4 matrices in the space of matrix representations of Lorentz transformations. We will use the next two sections to go over the virtual lepton flavor conservation and changing cases in greater detail.

2.3.1 Virtual lepton flavor conserving case

In this section, we will only look at the squared mass derivative method; it is the same procedure as explained in Section 2.2.1, but we must take $A = B$ into account. In particular, we will use Eqs. (2.6 - 2.13). Keep in mind that the auxiliary mass m_γ must be introduced into the propagator denominator.

After integrating the analytical expressions of the three diagrams over the four momentum k and taking the derivative twice with respect to squared-mass m_j^2, the $h_{m,1}^{AA}$, $h_{m,2}^{AA}$ and $h_{d,3}^{AA}$ functions are given by

$$h_{m,1}^{AA} = -\frac{e^3 v^2 \left(47m_A^2 - 8q^2\right)}{48\pi^2 m_A \left(q^2 - 4m_A^2\right)^2} B_1 + \frac{e^3 \mathrm{Qfi}^3 v^2 \left(10m_A^2 - q^2\right)}{6\pi^2 m_A \left(q^2 - 4m_A^2\right)^2} B_2 - \frac{11 e^3 m_A v^2}{16\pi^2 \left(q^2 - 4m_A^2\right)^2} B_3$$
$$- \frac{e^3 m_A v^2}{8\pi^2 m_A^2 - 2\pi^2 q^2} C_1 + \frac{e^3 v^2 \left(10m_A^3 - m_A q^2\right)}{2\pi^2 \left(q^2 - 4m_A^2\right)^2} C_2 - \frac{e^3 v^2 \left(124m_A^3 + 5m_A q^2\right)}{24\pi^2 \left(q^2 - 4m_A^2\right)^2} C_3$$
$$+ \frac{3e^3 m_A^3 v^2}{\pi^2 \left(q^2 - 4m_A^2\right)^2} C_4 - \frac{e^3 v^2 \left(68m_A^3 - 29m_A q^2\right)}{48\pi^2 \left(4m_A^2 - q^2\right)} D_1 - \frac{e^3 v^2 \left(68m_A^3 - 29m_A q^2\right)}{96\pi^2 \left(4m_A^2 - q^2\right)} D_2 + \frac{e^3 v^2}{8\pi^2 m_A^3},$$

$$(2.38)$$

$$h_{m,2}^{AA} = \frac{e^3 v^2 \left(47m_A^2 - 8q^2\right)}{48\pi^2 m_A \left(q^2 - 4m_A^2\right)^2} B_1 - \frac{e^3 v^2 \left(10m_A^2 - q^2\right)}{6\pi^2 m_A \left(q^2 - 4m_A^2\right)^2} B_2 + \frac{11 e^3 m_A v^2}{16\pi^2 \left(q^2 - 4m_A^2\right)^2} B_3 - \frac{5 e^3 m_A v^2}{24\pi^2 \left(4m_A^2 - q^2\right)} C_2$$
$$+ \frac{5 e^3 m_A v^2}{48\pi^2} D_1 + \frac{5 e^3 m_A v^2}{96\pi^2} D_2 + \frac{e^3 v^2}{16\pi^2 m_A^3},$$

$$(2.39)$$

$$h_{d,3}^{AA} = \frac{i e^3 v^2 m_A \left(m_A^2 \left(8x^2 - 4x(2y+1) + 4y^2 + 1\right) + q^2 \left(4x^4 - 8x^3 + 4x^2 + x(2y-1) - y^2\right)\right)}{8\pi^2 (x-y)^2 \left(4m_A^2 - q^2\right) \left(m_A^2 + q^2(x-1)x\right)} c_1$$
$$+ \frac{i e^3 v^2 (1 - 2y)^2 m_A}{8\pi^2 (x-y)^2 \left(4m_A^2 - q^2\right)} c_2 - \frac{i e^3 v^2 m_A}{8\pi^2 m_A^2 - 2\pi^2 q^2} c_3 - \frac{i e^3 v^2 (2x-1)(2y-1) m_A}{43\pi^2 (x-y)^2 \left(4m_A^2 - q^2\right)} c_4$$
$$- \frac{i e^3 v^2}{8\pi^2 m_A} c_5 + \frac{i e^3 v^2 (2x-1) m_A \left(4m_A^2 + q^2(2x-1)(2y-1)\right)}{8\pi^2 (x-y) \left(4m_A^2 - q^2\right)} d_1 + \frac{i e^3 v^2 m_A}{4\pi^2} d_2$$
$$- \frac{i e^3 v^2 (2y-1) m_A \left(4m_A^2 + q^2(2x-1)(2y-1)\right)}{8\pi^2 (x-y) \left(4m_A^2 - q^2\right)} d_3 - \frac{i e^3 v^2}{16\pi^2 m_A^3}.$$

$$(2.40)$$

The expressions for the PaVe scalar functions $B_1, B_2, B_3, C_1, C_2, C_3, C_4, D_1$ and D_2 for the magnetic form factor and $c_1, c_2, c_3, c_4, c_5, d_1, d_2$ and d_3 for the electric form factor are

$$B_1 = B_0 \left(0, m_A^2, m_A^2\right),$$
$$B_2 = B_0 \left(m_A^2, m_A^2, \mathrm{m}\gamma^2\right),$$
$$B_3 = B_0 \left(q^2, m_A^2, m_A^2\right),$$

$$C_1 = C_0 \left(0, 0, 0, m_A^2, m_A^2, m_A^2\right),$$
$$C_2 = C_0 \left(0, m_A^2, m_A^2, m_A^2, m_A^2, \mathrm{m}\gamma^2\right),$$
$$C_3 = C_0 \left(0, q^2, q^2, m_A^2, m_A^2, m_A^2\right),$$
$$C_4 = C_0 \left(m_A^2, m_A^2, q^2, m_A^2, \mathrm{m}\gamma^2, m_A^2\right),$$

$$D_1 = D_0 \left(0, 0, q^2, q^2, 0, q^2, m_A^2, m_A^2, m_A^2, m_A^2\right),$$
$$D_2 = D_0 \left(0, q^2, 0, q^2, q^2, q^2, m_A^2, m_A^2, m_A^2, m_A^2\right),$$

$$c_1 = C_0\left(0, -q^2x + q^2x^2 + m_A^2, -q^2x + q^2x^2 + m_A^2, m_A^2, m_A^2, m\gamma^2\right),$$

$$c_2 = C_0\left(0, -q^2y + q^2y^2 + m_A^2, -q^2y + q^2y^2 + m_A^2, m_A^2, m_A^2, m\gamma^2\right),$$

$$c_3 = C_0\left(0, q^2x^2 - 2q^2xy + q^2y^2, q^2x^2 - 2q^2xy + q^2y^2, m_A^2, m_A^2, m_A^2\right),$$

$$c_4 = C_0\left(-q^2x + q^2x^2 + m_A^2, -q^2y + q^2y^2 + m_A^2, q^2x^2 - 2q^2xy + q^2y^2, m_A^2, m\gamma^2, m_A^2\right),$$

$$c_5 = C_0\left(0, 0, 0, m_A^2, m_A^2, m_A^2\right),$$

$$d_1 = D_0\left(0, 0, m_A^2, -q^2x + q^2x^2 + m_A^2, 0, m_A^2, m_A^2, m_A^2, m_A^2, m\gamma^2\right),$$

$$d_2 = D_0\left(0, -q^2x + q^2x^2 + m_A^2, m_A^2, q^2x^2 - 2q^2xy + q^2y^2, -q^2x + q^2x^2 + m_A^2, q^2x^2 - 2q^2xy + q^2y^2, m_A^2, m_A^2, m\gamma^2, m_A^2\right),$$

$$d_3 = D_0\left(-q^2x + q^2x^2 + m_A^2, m_A^2, 0, q^2x^2 - 2q^2xy + q^2y^2, q^2x^2 - 2q^2xy + q^2y^2, m_A^2, m_A^2, m\gamma^2, m_A^2, m_A^2\right).$$

There are two key things to say. Because the expressions are shorter at this point, only the result after applying the squared-mass derivative and evaluating $m_j^2 = m_A^2$ is shown. The expression before applying the derivative has over two thousand terms, and it is impractical to show it. The other thing to notice about the expressions (2.38) and (2.39) is that they are independent of x. This is because the loop integrals of (2.11) and (2.13) are the same, but one has the factor x and the other $1 - x$. When we sum both of them, the x factor vanishes.

After parametric integrals shown in (2.38) - (2.40) are carried out, and the on shell condition $q^2 \to 0$ which defines the AMM and EDM contributions and $m_\gamma \to 0$ are implemented, the resulting virtual lepton flavor conserving expressions are

$$a_{\text{IR}}^{AA} = \frac{e^3v^2}{4\pi^2m_A^2}\text{tr}\left\{-\kappa_1^{AA}\left(\Delta_{\text{IR}} + \log\frac{\mu^2}{m_A^2}\right) + \frac{3}{8}(\kappa_2^{AA} - 5\kappa_1^{AA})\right\}, \tag{2.41}$$

$$d_{\text{IR}}^{AA} = \frac{ie^3v^2}{16\pi^2m_A^3}\text{tr}\left\{-2\kappa_3^{AA}\left(\Delta_{IR} + \log\frac{\mu^2}{m_A^2}\right) + 3\kappa_3^{AA}\right\}. \tag{2.42}$$

The presence of IR divergences in the EMMs is explicitly given by the factor $\Delta_{\text{IR}} + \log\frac{\mu^2}{m_A^2}$ and results from the virtual photon inside the loop, so these quantities are not observables. However, we will discuss in the next section how such divergences are expected to disappear from some cross section. Keeping this in mind, we instead aim to estimate the effects of the finite parts of these quantities on some physical observable, for which we omit the divergent terms in the following.

$$a_{l_A}^{AA} = \frac{e^3v^2}{4\pi^2m_A^2}\text{tr}\left\{\frac{3}{8}(\kappa_2^{AA} - 5\kappa_1^{AA})\right\}, \tag{2.43}$$

$$d_{l_A}^{AA} = \frac{ie^3v^2}{16\pi^2m_A^3}3\text{tr}\kappa_3^{AA}. \tag{2.44}$$

On the other hand, UV divergences introduced by each contributing loop diagram lie exclusively within two point scalar functions B_0. Using the dimensional regularization approach [111], any scalar function B_0 can be written in form

$$B_0 = \Delta_{\text{UV}} + \text{(finite terms)}, \tag{2.45}$$

where

$$\Delta_{\text{UV}} = \frac{1}{\varepsilon} - \gamma_E + \log \frac{4\pi}{\mu^2}, \tag{2.46}$$

diverges as $\varepsilon = 4 - D \to 0$ [112]. All B_0 functions share the same UV-divergent term Δ_{UV}, so any difference of the form $B_0^j - B_0^k$, with B_0^j and B_0^k denoting different two point scalar functions, is free of UV divergences. To make the preceding statement clearer, we rewrite $h_{d,1}^{AA}$ and $h_{d,2}^{AA}$ from the AMM as follows

$$h_{d,1}^{AA} = f_1(B_1 - B_2) + (f_1 + f_2)(B_2 - B_3) + (f_1 + f_2 + f_3)B_3, \tag{2.47}$$

$$h_{d,2}^{AA} = g_1(B_1 - B_2) + (g_1 + g_2)(B_2 - B_3) + (g_1 + g_2 + g_3)B_3, \tag{2.48}$$

the scalar functions $f_{1,2,3}$ and $g_{1,2,3}$ are those, in Eqs. (2.38) and (2.39), that multiply the PaVe scalar functions $B_{1,2,3}$ respectively. We can easily verify that the final terms proportional to B_3 are equal to zero. This ensures that a^{AA} is UV finite because we can express it in terms of the differences $B_1 - B_2$ and $B_2 - B_3$. The EDM, d^{AA} is UV finite by its own because it is not a function of two point scalar functions B_0.

Infrared divergences

From a mathematical standpoint, we can see that IR divergences appear when a particle has no mass; for example, the electron self energy expression is

$$\int \frac{d^4k}{(2\pi^4)} \gamma^\mu \frac{i(\slashed{q} - \slashed{k} + m)}{(q - k)^2 - m^2 + i\varepsilon} \gamma^\mu \frac{1}{k^2}, \tag{2.49}$$

we can see that in the limit as $k \to 0$ the integral goes to infinity.

Adding a regulator is a method for removing the IR divergence. In this case, we could, for example, include a photon mass m_γ [97–101]. When we introduce this fictitious photon mass, the singularity vanishes

$$\int \frac{d^4k}{(2\pi^4)} \gamma^\mu \frac{i(\slashed{q} - \slashed{k} + m)}{(q - k)^2 - m^2 + i\varepsilon} \gamma^\mu \frac{1}{k^2 - m_\gamma^2}. \tag{2.50}$$

This mass was added to make the loops finite, and it is an example of an IR regulator. The use of IR regulators is manifested not through differences in Green's functions at different scales (as with UV regulators), but through the sum of different types of Green's functions contributing to the same observable at the same scale.

Because virtual photon diagrams, shown in Fig. (2.3), are associated with IR divergences, we propose a fictitious photon mass, m_γ too. A point worth noting is that diagrams with two point insertions on a single virtual fermion line produce IR divergences, as shown in the last two diagrams in Fig. (2.3), whereas an IR finite diagram has exactly one such insertion in the lepton propagators.

For a moment, consider in the context of the Lorentz invariant QED, the electromagnetic vertex $A_\mu l_A l_A$ at one loop. The contributions from quantum electrodynamics to this vertex are parametrized as

$$= ie \left[\gamma_\mu F_1(q^2) + i\sigma_{\mu\nu} q^\nu \frac{F_2(q^2)}{2m_l} \right]. \tag{2.51}$$

Whereas the electric form factor $F_1(q^2)$ involves both UV and IR divergences, the magnetic form factor $F_2(q^2)$ is finite in both senses.

The IR divergences can be seen as arising from the incomplete consideration of all the factors in a cross section. An arbitrary number of soft photons may exist in the final state. That is, IR divergences are removed at the cross section level rather than directly from the amplitude of this contribution.

So, it can be shown that even though $l_A^+ l_A^- \to l_B^+ l_B^-$ is IR divergent and so is $l_A^+ l_A^- \to l_B^+ l_B^- \gamma$, their sum is IR finite. For this, consider the QED contributions to the process $l_A^+ l_A^- \to l_B^+ l_B^-$, the amplitude can be written as

$$\mathcal{M}_{2\to 2} = \mathcal{M}_{2\to 2}^{\text{tree}} + \mathcal{M}_{2\to 2}^{\text{loop}}, \tag{2.52}$$

the first and second terms correspond to the tree level and loop contributions, respectively. We can express the loop amplitude contribution in a more convenient way

$$\mathcal{M}_{2\to 2}^{\text{loop}} = \mathcal{M}_{2\to 2}^{\gamma l_A l_A} + ..., \tag{2.53}$$

where the ellipsis represents the four missing relevant one-loop graphs in QED [101]. The vertex correction, $\mathcal{M}_{2\to 2}^{\gamma l_A l_A}$, is

$$\mathcal{M}_{2\to 2}^{\gamma l_A l_A} = \qquad + \qquad . \tag{2.54}$$

The second diagram in Eq. (2.54), representing the counterterm for the first one, is introduced as part of the renormalization procedure.

Differential cross section contribution of interference terms

$$d\sigma_v = d\sigma_{2\to 2}^{\text{interf}} \propto \sum_{\text{spin}} \left[\left(\mathcal{M}_{2\to 2}^{\text{tree}} \right)^* \mathcal{M}_{2\to 2}^{\gamma l_A l_A} + \mathcal{M}_{2\to 2}^{\text{tree}} \left(\mathcal{M}_{2\to 2}^{\gamma l_A l_A} \right)^* \right]. \tag{2.55}$$

where σ_v, the virtual cross section correction at order e_R^6, still exhibits IR divergences.

$$\sigma_V = \frac{e_R^2}{8\pi^2} \sigma_0 \left(-\ln^2 \frac{m_\gamma^2}{Q^2} - 3\ln \frac{m_\gamma^2}{Q^2} - \frac{7}{2} + \frac{\pi^2}{3} \right), \tag{2.56}$$

$\sigma_0 = e_R^4/12\pi Q^2$ and Q^2 is the photon momentum entering the vertex. The squared logarithm is characteristic of IR divergences and is called the **Sudakov double logarithm**.

As we will see, the resolution is such that a cross section is not an observable: only by including contributions from the process with different final states can we find an observable that is independent of m_γ.

Next, we calculate the cross section for bremsstrahlung process, $l_A^+ l_A^- \to \gamma l_A^+ l_A^-$ under the assumption that the final state photon is soft. The tree level amplitude is expressed as $\mathcal{M}_{2\to 3}^{\text{tree}} = \mathcal{M}_{2\to 3}^{\gamma l_A l_A} + ...$, where

$$\mathcal{M}_{2\to 3}^{\gamma l_A l_A} = \quad \text{} \quad + \quad \text{} \quad . \tag{2.57}$$

The corresponding differential cross section is

$$d\sigma_{2\to 3} = d\sigma_{2\to 3}^{\gamma l_A l_A} + ..., \tag{2.58}$$

with

$$d\sigma_{2\to 3}^{\gamma l_A l_A} \propto \sum_{\text{spin}} |\mathcal{M}_{2\to 3}^{\gamma l_A l_A}|^2. \tag{2.59}$$

Skipping details of the derivation [101], the real emission diagrams give,

$$\sigma_R = \frac{e_R^2}{8\pi^2} \sigma_0 \left(\ln^2 \frac{m_\gamma^2}{Q^2} + 3\ln \frac{m_\gamma^2}{Q^2} + 5 - \frac{\pi^2}{3} \right), \tag{2.60}$$

anticipating the IR divergence, the calculation was regulated with a photon mass.
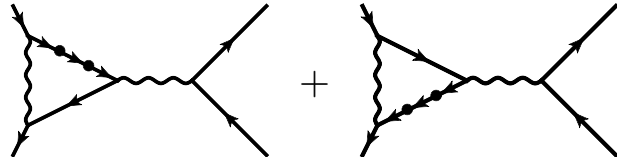
We see that all IR divergent terms precisely cancel, from Eqs. (2.60) and (2.56) we are left with

$$\sigma_R + \sigma_V = \frac{3e_R^2}{16\pi^2}\sigma_0. \tag{2.61}$$

As a result, when we consider both the virtual contribution and the real emission, the IR divergences cancel. It is also worth noting that the bremsstrahlung diagrams of Eq. (2.57) are created by inserting the electromagnetic vertex only proportional to γ_μ in an external line of some tree level diagram $l_A l_A \to l_B l_B$. This is the same Dirac matrix that appears in the IR-divergent form factor $F_1(q^2)$ in Eq. (2.51).
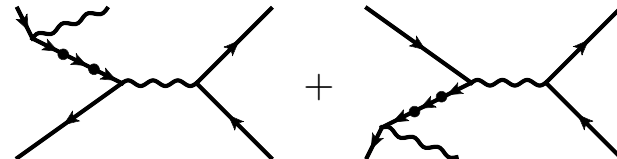
In the case of the mSME contributions considered for this study, IR divergences arise in the magnetic and electric form factors proportional to 4×4 matrices $\sigma_{\mu\nu}$ and $\sigma_{\mu\nu}\gamma_5$, respectively, defined in the space of Dirac matrices. This means that such factors are not measurable. We argue that, similarly to the SM Lorentz conserving case, such IR divergences should vanish at the cross section level, with the help of bremsstrahlung diagrams containing Lorentz-violating bilinear insertions.

Analogously to the case explained before, consider the one loop Lorentz violating amplitude of $l_A l_A \to l_B l_B$, which, among the whole set of contributing Feynman diagrams, receives contributions from the IR divergent sum

$$\tag{2.62}$$

The bremsstrahlung diagrams, which bear the effects of Lorentz invariance violation caused by SME bilinear insertions, contribute to $l_A l_A \to \gamma l_B l_B$ at the tree level:

$$\tag{2.63}$$

A soft photon final state is assumed as well. Both sums of diagrams (2.62) and (2.63) are IR divergent. The part proportional to matrices $\sigma_{\mu\nu}$ and $\sigma_{\mu\nu}\gamma_5$ are expected to contribute to differential cross sections that, when added together, should cancel out all IR divergences, yielding a finite total cross section. The verification of this statement is the goal of a future ongoing investigation.

2.3.2 Virtual lepton flavor changing case

In this case, we consider lepton flavor change within the loop, which means $m_B \neq m_A$. We will concentrate on the procedure that includes the five propagators and calculation of four- and five-point PaVe scalar functions; this problem was solved using Package X. It is difficult to write all the terms that appear when we make the loop integral; the magnetic form factor contains approximately 6,000 terms, while the electric form factor contains approximately 4,000 terms; however, in general, they can be written as follows.

$$f_m^{AB} = w_{m,1}^{AB} A_1 + w_{m,2}^{AB} A_2 + w_{m,3}^{AB} A_3 + w_{m,4}^{AB} B_1 + w_{m,5}^{AB} B_2 + w_{m,6}^{AB} B_3 + w_{m,7}^{AB} B_4 + w_{m,8}^{AB} B_5$$
$$+ w_{m,9}^{AB} C_1 + w_{m,10}^{AB} C_2 + w_{m,11}^{AB} C_3 + w_{m,12}^{AB} C_4 + w_{m,13}^{AB} C_5 + w_{m,14}^{AB} D_1, \tag{2.64}$$

$$f_d^{AB} = w_{d,1}^{AB} A_1 + w_{m,2}^{AB} A_2 + w_{m,3}^{AB} B_1 + w_{m,4}^{AB} B_2 + w_{m,5}^{AB} B_3 + w_{m,6}^{AB} B_4 + w_{m,7}^{AB} B_5$$
$$+ w_{m,8}^{AB} C_1 + w_{m,9}^{AB} C_2 + w_{m,10}^{AB} C_3 + w_{m,11}^{AB} C_4 + w_{m,12}^{AB} C_5 + w_{m,13}^{AB} D_1, \tag{2.65}$$

$$\tag{2.66}$$

where

$$A_1 = A_0(m_A^2),$$
$$A_2 = A_0(m_B^2),$$

$$B_1 = B_0(q^2, m_A^2, m_A^2),$$
$$B_2 = B_0(q^2, m_B^2, m_B^2),$$
$$B_3 = B_0(q^2, m_A^2, m_B^2),$$
$$B_4 = B_0(m_A^2, m_A^2, m_\gamma^2),$$
$$B_5 = B_0(m_A^2, m_B^2, m_\gamma^2),$$

$$C_1 = C_0(m_A^2, m_A^2, 0, m_A^2, m_\gamma^2, m_A^2),$$
$$C_2 = C_0(0, q^2, q^2, m_A^2, m_A^2, m_A^2),$$
$$C_3 = C_0(m_A^2, m_A^2, q^2, m_A^2, m_\gamma^2, m_A^2),$$
$$C_4 = C_0(m_A^2, m_A^2, q^2, m_B^2, m_\gamma^2, m_B^2),$$
$$C_5 = C_0(m_A^2, m_A^2, q^2, m_A^2, m_\gamma^2, m_B^2)$$

$$D_1 = D_0(m_A^2, m_A^2, 0, q^2, q^2, m_A^2, m_A^2, m_\gamma^2, m_A^2, m_A^2).$$

The scalar functions $w_{m,i}^{AB} = w_{m,i}^{AB}(\text{tr}\kappa_1^{AB}, \text{tr}\kappa_2^{AB}, m_A, m_B, m_\gamma, q^2)$ with $i = 1, ..., 14$, and $w_{d,j}^{AB} = (\text{tr}\kappa_3^{AB}, m_A, m_B, m_\gamma, q^2)$ with $j = 1, ..., 13$.

After solving the PaVe scalar function, the AMM and EDM are

$$
\begin{aligned}
a^{AB} =& \frac{e^3 v^2}{192\pi^2 m_A^7 (m_A^2 - m_B^2)^2} \operatorname{tr}\left\{ (\kappa_1^{AB} - \kappa_2^{AB}) \left(34 m_A^8 \log\frac{m_A^2}{m_B^2} + (m_A^2 - m_B^2)\left(-13 m_A^4 m_B^2 + 18 m_A^2 m_B^4 \right.\right.\right. \\
& \left.\left. + 2(-19 m_A^4 m_B^2 + 11 m_A^2 m_B^4 + 17 m_A^6 - 9 m_B^6) \log\frac{m_B^2}{m_B^2 - m_A^2} - 39 m_A^6 \right)\right) - 24 m_A^3 m_B (\kappa_1^{AB} + \kappa_2^{AB}) \\
& \left. \left(m_A^4 \log\frac{m_A^2}{m_B^2} + (m_A^2 - m_B^2)\left(2\left(m_A^2 - m_B^2 \right) \log\frac{m_B^2}{m_B^2 - m_A^2} - m_A^2 \right) \right) \right\},
\end{aligned}
\tag{2.67}
$$

$$
d^{AB} = \frac{i e^3 v^2 m_B^3}{4\pi^2 m_A^4 (m_A^2 - m_B^2)} \left(\log\frac{m_B^2}{m_B^2 - m_A^2} + \frac{m_A^2}{2 m_B^2}\left(\Delta_{\text{IR}} + \log\frac{\mu^2}{m_A^2} \right) \right) \operatorname{tr}\kappa_3^{AB}.
\tag{2.68}
$$

The corresponding contributions to AMMs are free of both UV and IR divergences, whereas the resulting EDMs turn out to be IR divergent. After removing such IR divergences, the virtual lepton flavor changing contributions to AMMs and EDMs are expressed as

$$
\begin{aligned}
a_{l_A}^{AB} =& \frac{e^3 v^2}{192\pi^2 m_A^7 (m_A^2 - m_B^2)^2} \operatorname{tr}\left\{ (\kappa_1^{AB} - \kappa_2^{AB}) \left(34 m_A^8 \log\frac{m_A^2}{m_B^2} + (m_A^2 - m_B^2)\left(-13 m_A^4 m_B^2 + 18 m_A^2 m_B^4 \right.\right.\right. \\
& \left.\left. + 2(-19 m_A^4 m_B^2 + 11 m_A^2 m_B^4 + 17 m_A^6 - 9 m_B^6) \log\frac{m_B^2}{m_B^2 - m_A^2} - 39 m_A^6 \right)\right) - 24 m_A^3 m_B (\kappa_1^{AB} + \kappa_2^{AB}) \\
& \left. \left(m_A^4 \log\frac{m_A^2}{m_B^2} + (m_A^2 - m_B^2)\left(2\left(m_A^2 - m_B^2 \right) \log\frac{m_B^2}{m_B^2 - m_A^2} - m_A^2 \right) \right) \right\},
\end{aligned}
\tag{2.69}
$$

$$
d_{l_A}^{AB} = \frac{i e^3 v^2 m_B^3}{4\pi^2 m_A^4 (m_A^2 - m_B^2)} \log\frac{m_B^2}{m_B^2 - m_A^2} \operatorname{tr}\kappa_3^{AB}.
\tag{2.70}
$$

The resulting electromagnetic contributions come from the sum of the Eqs. (2.43) and (2.69) for the AMM, and (2.44) plus (2.70) for the EDM. The total contributions can be organized as

$$
a_{l_A}^{\text{SME}} = \sum_{j=1}^{2} \sum_{B=e,\mu,\tau} a_j^{AB} \operatorname{tr}\kappa_j^{AB},
\tag{2.71}
$$

$$
d_{l_A}^{\text{SME}} = \sum_{B=e,\mu,\tau} d_3^{AB} \operatorname{tr}\kappa_3^{AB}.
\tag{2.72}
$$

Chapter 3

Estimations and discussion

The goal of this chapter is to estimate bounds on SME coefficients from the Yukawa sector given in Eq. (1.15). In order to reduce the number of parameters, we consider scenarios defined by specific assumptions on Lorentz non conserving coefficients, about which we will talk later.

The intrinsic magnetic moments of elementary particles, which gave rise to the concept of spin, are subjected to quantum corrections known as AMMs [113]. The difference between the SM contribution to the AMM of some fermion f, a_f^{SM}, and the best experimental measurement currently available, a_f^{exp} is conventionally characterized by the quantity

$$\Delta a_f = a_f^{\mathrm{exp}} - a_f^{\mathrm{SM}}. \tag{3.1}$$

These discrepancies being so tiny can be interpreted as suitable places to look for suppressed *new physics* beyond the SM.

Anomalous magnetic moment bounds

- In the cases of the electron and the muon AMMs, the corresponding SM predictions have been calculated and estimated with remarkable precision [114, 115] whereas experimental studies have reached exceptional sensitivity [116–118].

For the electron AMM

$$\Delta a_e = -1.06(082) \times 10^{-12}, \tag{3.2}$$

has been reported [114].

For the muon case [115]

35

$$\Delta a_\mu = 249(87) \times 10^{-11}. \tag{3.3}$$

- The much less well known tau lepton AMM was investigated by the authors of Ref. [13], who analyzed collider data and then determined model independent limits on new physics contributions to this quantity.

$$-0.007 < a_\tau^{\mathrm{NP}} < 0.005 \tag{3.4}$$

Electric dipole moment bounds

The EDMs of elementary particles have not been measured ever, so our best experimental knowledge on the matter consists in bounds.

- The electron EDM d_e has particularly stringent limits. Experiments with Thallium atoms and Ytterbium fluoride molecules yielded high sensitivities, resulting in upper bounds on $|d_e|$ of order $10^{-27} e \cdot cm$ [119–121]. In addition, the ACME Collaboration reported an improved upper limit at 90% C.L. [122, 123]

$$|d_e| < 8.7 \times 10^{-29} e \cdot cm. \tag{3.5}$$

- Three analyses aimed at the observation of the muon EDM were performed and reported in Ref. [124] by the Muon $g-2$ Collaboration. This group concluded that the lack of any signal yields the bound, at 95 % C.L.

$$|d_\mu| < 1.8 \times 10^{-19} e \cdot cm. \tag{3.6}$$

- An experimental investigation carried out by the Belle Collaboration searched for CP violation induced by the tau lepton EDM, determining at 95% C.L. the limits [125]

$$-2.2 \times 10^{-17} e \cdot cm < \mathrm{Re}(d_\tau) < 4.5 \times 10^{-17} e \cdot cm, \tag{3.7}$$

$$-2.5 \times 10^{-17} e \cdot cm < \mathrm{Im}(d_\tau) < 0.8 \times 10^{-17} e \cdot cm. \tag{3.8}$$

We use Eqs. (2.71) and (2.72) in order to determine bounds.

3.1 Real and imaginary AMM and EDM

Following Ref. [126] we assume that matrices $V_{\alpha\beta}$ and $A_{\alpha\beta}$ are symmetric in flavor space. Remember that these matrices are Hermitian and anti Hermitian, respectively, leading to the conclusion:

- $V_{\alpha\beta}$ are real,

- $A_{\alpha\beta}$ are imaginary.

Therefore, according to the definitions shown in Eqs. (2.17)-(2.19)

- $\operatorname{tr}\kappa_1^{AB}$ and $\operatorname{tr}\kappa_2^{AB}$ are real,

- $\operatorname{tr}\kappa_3^{AB}$ is imaginary.

These properties are crucial because observing the structure of $a_{l_A}^{AA}$ and $d_{l_A}^{AA}$, in Eqs. (2.43) and (2.44), allows us to conclude that both virtual lepton flavor conserving contributions to EMMs are real. This seems to be plausible because, in general, we can consider some kind of new physics generating contributions to the magnetic and/or electric form factors of fermions. The resulting set of electromagnetic form factors can be divided [104, 105] into the following categories:

- *Diagonal electromagnetic form factors*, in which external fermions coincide with each other, $A_\mu f_A f_A$. This is the case under consideration in this thesis.

- *Transition electromagnetic form factors*, characterized by different external fermions, $A_\mu f_A f_B$.

If transitions between leptons and quarks are forbidden, each of these fermion types produces nine magnetic moments and nine electric moments, with each set arranged as a 3×3 matrix. All such matrices, whose diagonal entries are the diagonal moments and whose transition moments act as nondiagonal components, are conventionally assumed to be Hermitian, which means that diagonal moments are real but transition moments can be complex.

On the other hand, working with the vertex $A_\mu f_A f_A$ off shell may introduce thresholds beyond which imaginary parts of diagonal moments may be induced. It turns out that, despite the fact that AMMs and EDMs are on shell quantities, electromagnetic moments of unstable particles can have imaginary parts. The authors of Ref. [127] argued that AMMs and EDMs are guaranteed to be real only when calculated in the context of Lorentz conserving QED, and they suggested that ad hoc definitions of these electromagnetic properties should be provided in more general situations. A two loop calculation included in their discussion demonstrated that even the SM produces complex AMMs and EDMs. Complex electromagnetic moments has also been mentioned in Refs. [128, 129].

From the explicit expressions provided in Eqs. (2.69) and (2.70) notice that Lorentz non conserving contributions to charged lepton AMMs and EDMs could be complex, despite the fact that these electromagnetic moments are not transition like, but rather diagonal moments, and given the fact that they were calculated on shell. The presence of the logarithm $\log \frac{m_B^2}{m_B^2 - m_A^2}$ causes this behavior, it is real if $m_B > m_A$ or imaginary if $m_A > m_B$. The graphs in Figs. (3.1) and (3.2) show how the real and imaginary parts of coefficients a_1^{AB}, a_2^{AB} and d_3^{AB} behave, these are the scalar functions, in terms of the virtual lepton mass m_B, that multiply $\operatorname{tr}\kappa_1^{AB}$, $\operatorname{tr}\kappa_2^{AB}$, for AMM contribution, and $\operatorname{tr}\kappa_3^{AB}$, for EDM contribution, respectively. It is only shown for the case $A = \mu$ corresponding to external muons, but we have made sure that an analogous behavior occurs if external leptons l_e and l_τ are considered.

In these graphs, short dashed curves (brown or purple) represent the **real parts** of coefficients $a_j^{\mu B}$, with $j = 1, 2, 3$, while long dashed plots (red or orange) depict **imaginary parts** of such quantities. Horizontal solid lines represent the values $a_j^{\mu B} = 0$. Vertical solid lines are located at value of the muon mass m_μ, corresponding to a m_B threshold. Near this line the factors $a_j^{\mu B}$ are either complex or only real or imaginary quantities.

Both graphs, of AMM, make it evident that the values of l_B mass such that $m_B < m_\mu$ yield real and imaginary contributions, whereas these contributions are only real as long as $m_B > m_\mu$. In the case of EDM, for $m_B < m_\mu$ the contribution has real and imaginary parts too, whereas the real part vanishes for $m_B > m_\mu$, but its imaginary part remains nonzero. Because the trace $tr \kappa_3^{\mu B}$ is purely imaginary, a global imaginary factor from this trace should be sufficient to get things right.

In a general context, imaginary parts of one loop amplitudes, if present, usually emerge when some external field is connected to loop lines corresponding to particles which together are lighter than the external particle. In the case of the Lorentz violating theory considered in the present investigation, the insertion of bilinear vertices connecting some external field line to a lighter virtual field line produces a similar effect.

3.2 Textures

Consider the following 3×3 matrices

$$\chi_j = \begin{pmatrix} \chi_j^{ee} & \chi_j^{e\mu} & \chi_j^{e\tau} \\ \chi_j^{\mu e} & \chi_j^{\mu\mu} & \chi_j^{\mu\tau} \\ \chi_j^{\tau e} & \chi_j^{\tau\mu} & \chi_j^{\tau\tau} \end{pmatrix} \equiv \begin{pmatrix} \operatorname{tr} \kappa_j^{ee} & \operatorname{tr} \kappa_j^{e\mu} & \operatorname{tr} \kappa_j^{e\tau} \\ \operatorname{tr} \kappa_j^{\mu e} & \operatorname{tr} \kappa_j^{\mu\mu} & \operatorname{tr} \kappa_j^{\mu\tau} \\ \operatorname{tr} \kappa_j^{\tau e} & \operatorname{tr} \kappa_j^{\tau\mu} & \operatorname{tr} \kappa_j^{\tau\tau} \end{pmatrix}. \tag{3.9}$$

These matrices have nothing to do with transition electromagnetic moments, which have different flavors for external fermions. They only correspond to diagonal electromagnetic moments and instead characterize the terms of such quantities in which virtual lepton flavor is preserved or changed.

According to Eqs. (2.71) and (2.72), the contributions from Lorentz violation coefficients to the AMM of leptons are

$$a_e^{\mathrm{SME}} = \sum_{j=1}^{2} (a_j^{ee} \chi_j^{ee} + a_j^{e\mu} \chi_j^{e\mu} + a_j^{e\tau} \chi_j^{e\tau}),$$

$$a_\mu^{\mathrm{SME}} = \sum_{j=1}^{2} (a_j^{\mu e} \chi_j^{\mu e} + a_j^{\mu\mu} \chi_j^{\mu\mu} + a_j^{\mu\tau} \chi_j^{\mu\tau}),$$

$$a_\tau^{\mathrm{SME}} = \sum_{j=1}^{2} (a_j^{\tau e} \chi_j^{\tau e} + a_j^{\tau\mu} \chi_j^{\tau\mu} + a_j^{\tau\tau} \chi_j^{\tau\tau}). \tag{3.10}$$

The EDM are

Figure 3.1: Factor of traces in muon AMM, $a_{l_\mu}^{\mu B}$, shown in Eq. (2.69), as function of the virtual lepton mass m_B. The upper graph displays $a_1^{\mu B}$, the coefficient of $\mathrm{tr}\kappa_1^{\mu B}$, while $a_2^{\mu B}$, the coefficient of $\mathrm{tr}\kappa_2^{\mu B}$ is shown in the lower graph.

$$d_e^{\mathrm{SME}} = a_3^{ee}\chi_3^{ee} + a_3^{e\mu}\chi_3^{e\mu} + a_3^{e\tau}\chi_3^{e\tau},$$

$$d_\mu^{\mathrm{SME}} = a_3^{\mu e}\chi_3^{\mu e} + a_3^{\mu\mu}\chi_3^{\mu\mu} + a_3^{\mu\tau}\chi_3^{\mu\tau},$$

$$d_\tau^{\mathrm{SME}} = a_3^{\tau e}\chi_3^{\tau e} + a_3^{\tau\mu}\chi_3^{\tau\mu} + a_3^{\tau\tau}\chi_3^{\tau\tau}. \tag{3.11}$$
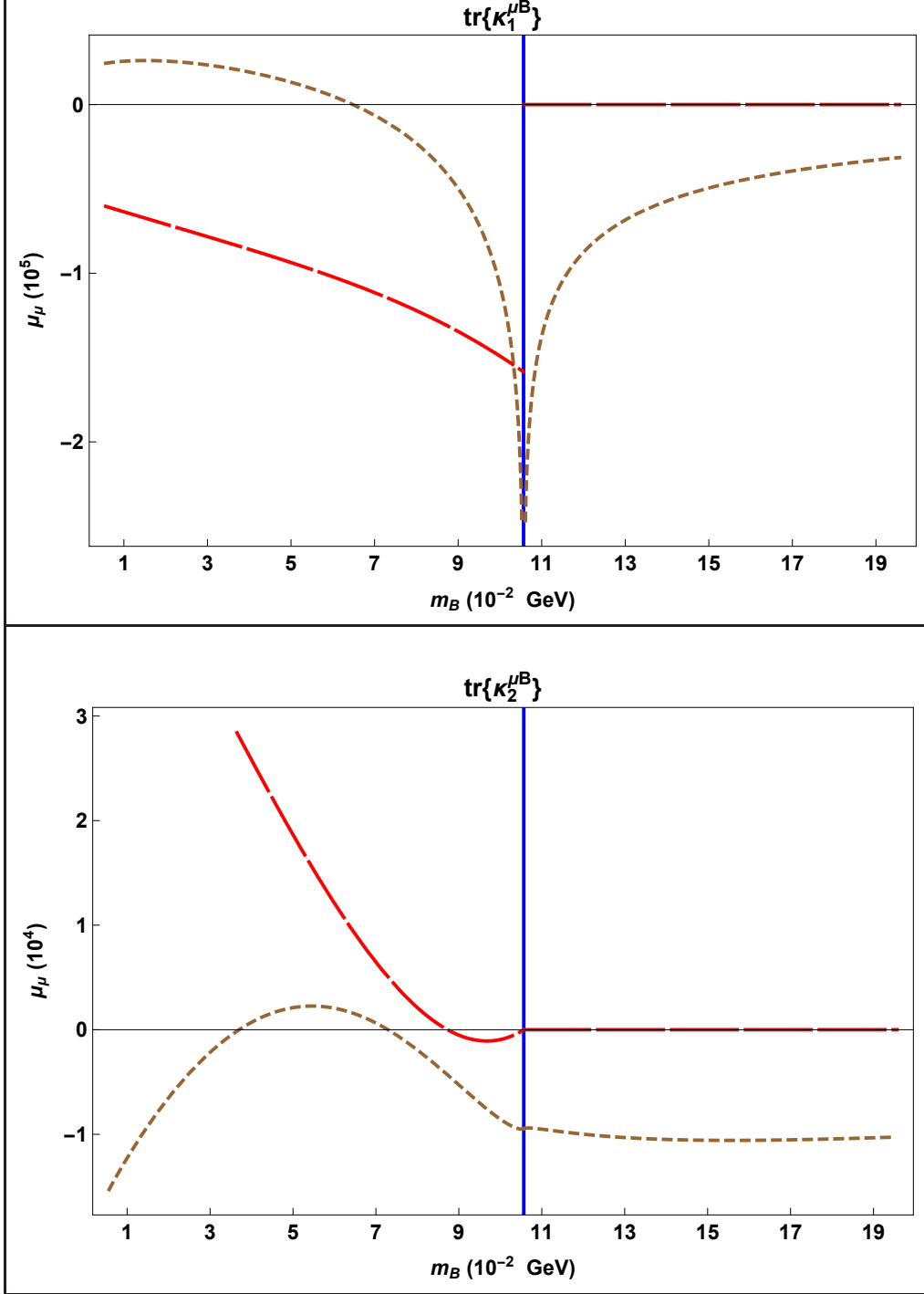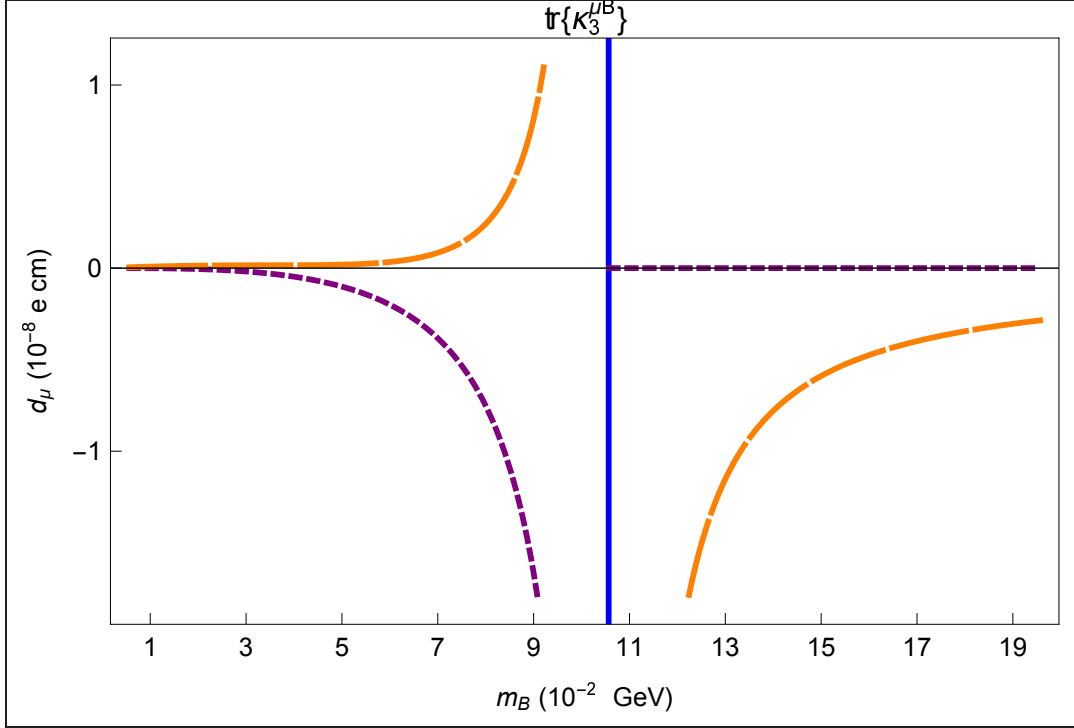
Figure 3.2: Factor of trace in muon EDM, $d_{l_\mu}^{\mu B}$, shown in Eq. (2.70), as function of the virtual lepton mass m_B. The graph displays $a_3^{\mu B}$, the coefficient of $\mathrm{tr}\kappa_3^{\mu B}$.

Notice that the first rows of matrices χ_1, χ_2 and χ_3 comprise all the SME traces $\chi_j^{eB} = \mathrm{tr}\kappa_j^{eB}$ necessary to determine the electron AMM and EDM contribution. The same is true for the second and third rows of the matrices χ_j, which determine the muon and tau AMMs and EDMs, respectively. Remember that matrices χ_1, χ_2 contribute to the AMMs, whereas χ_3 contribute to the EDMs of the leptons $l_{e,\mu,\tau}$.

We demonstrate the following properties using equations (2.22)-(2.24)

$$\chi_1^\dagger = \chi_1, \qquad \chi_2^\dagger = \chi_2, \tag{3.12}$$

$$\chi_3^\dagger = -\chi_3. \tag{3.13}$$

That is, not of all the traces defining the entries of matrices χ_j are independent. Furthermore, the previous assumption that $V_{\alpha\beta}^{AB} = V_{\alpha\beta}^{BA}$ and $A_{\alpha\beta}^{AB} = A_{\alpha\beta}^{BA}$ guarantees that χ_1 and χ_2 are symmetric and real, whereas χ_3 is symmetric and imaginary. Thus, each matrix χ_j is determined by six independent parameters χ_j^{AB}. Since AMM contributions are given exclusively in terms of χ_1 and χ_2 these quantities are determined by $6 \times 2 = 12$ real traces, whereas EDMs expressed only in terms if χ_3 involve 6 independent traces in total.

With these definitions at hand, we can think about scenarios distinguished by matrix textures.

3.2.1 Quasidiagonal textures

This scenario is defined by the assumption that the diagonal entries of matrices χ_j are by far dominant, whereas off-diagonal components of such matrices are practically equal zero, that is $\chi_j^{AB} \approx 0$ for $A \neq B$. Then, χ_j matrices look like

$$\chi_j \approx \begin{pmatrix} \chi_j^{ee} & 0 & 0 \\ 0 & \chi_j^{\mu\mu} & 0 \\ 0 & 0 & \chi_j^{\tau\tau}, \end{pmatrix} \tag{3.14}$$

So, Eqs. (3.10) and (3.11) are expressed as

$$a_{l_A}^{\text{SME}} \approx a_1^{AA}\chi_1^{AA} + a_2^{AA}\chi_2^{AA}, \tag{3.15}$$

$$d_{l_A}^{\text{SME}} \approx d_3^{AA}\chi_3^{AA}, \tag{3.16}$$

the repeated flavor indices mean virtual lepton flavor conserving.

In this way we could determine a mSME contribution to AMM $a_{l_A}^{\text{SME}}$ only by two parameters, $(\chi_1^{AA}, \chi_2^{AA})$, whereas the mSME contribution EDM is given by only one, χ_3^{AA}.

The parameter regions in $(\chi_1^{AA}, \chi_2^{AA})$ space allowed by the current constraints from beyond-SM physics on AMM are obtained using Eqs. (3.2 - 3.4) as follows

$$|a_1^{AA}\chi_1^{AA} + a_2^{AA}\chi_2^{AA}| < |\Delta a_{l_A}|. \tag{3.17}$$

Figures (3.3 - 3.5) display this allowed region for the case of SME contributions to the electron, muon and tau AMM after choosing specific intervals for χ_1 and χ_2:

- For electron; $|\chi_1^e| < 0.73 \times 10^{-21}$ and $|\chi_2^e| < 1 \times 10^{-21}$.

- For muon; $|\chi_1^\mu| < 0.74 \times 10^{-13}$ and $|\chi_2^\mu| < 1 \times 10^{-13}$.

- For tau; $|\chi_1^\tau| < 0.5 \times 10^{-4}$ and $|\chi_2^\tau| < 1 \times 10^{-4}$.

Figure (3.3) shows that the Lorentz violation coefficient χ_1^{ee} is more restricted than χ_2^{ee}. For any value of χ_2^{ee}, the trace χ_1^{ee} lies within a narrow interval of width $\approx 10.5189 \times 10^{-22}$. Moreover, as long as Lorentz violation traces χ_2^{ee} of order $\lesssim 10^{-21}$ are assumed, the value of χ_1^{ee} is more likely to be negative.

From (3.4) we can observe that the trace $\chi_1^{\mu\mu}$ lies within a narrow interval of width $\approx 10.63 \times 10^{-14}$ and traces $\chi_2^{\mu\mu}$ of order $\lesssim 10^{-13}$ are assumed.

Figure 3.3: The allowed region within the parameter space (χ_1^e, χ_2^e), for quasidegenerate texture, for $|\chi_1^e| < 0.73 \times 10^{-21}$ and $|\chi_2^e| < 10^{-21}$. We have denoted $\chi_1^{ee} = \chi_1^e$

Figure 3.4: The allowed region within the parameter space (χ_1^μ, χ_2^μ), for quasidegenerate texture, for $|\chi_1^\mu| < 0.74 \times 10^{-13}$ and $|\chi_1^\mu| < 10^{-13}$. We have denoted $\chi_1^{\mu\mu} = \chi_1^\mu$

We can deduce from (3.5) that the Lorentz violation coefficients $\chi_1^{\tau\tau}$ are more restricted than $\chi_2^{\tau\tau}$ as the electron and muon cases, but note that the shadowed region is wider that the others, indicating that $\chi_1^{\tau\tau}$ is less suppressed than the other leptons.

The table (3.6) contains data for all the leptons. The first rows show the minimum (bottom) and
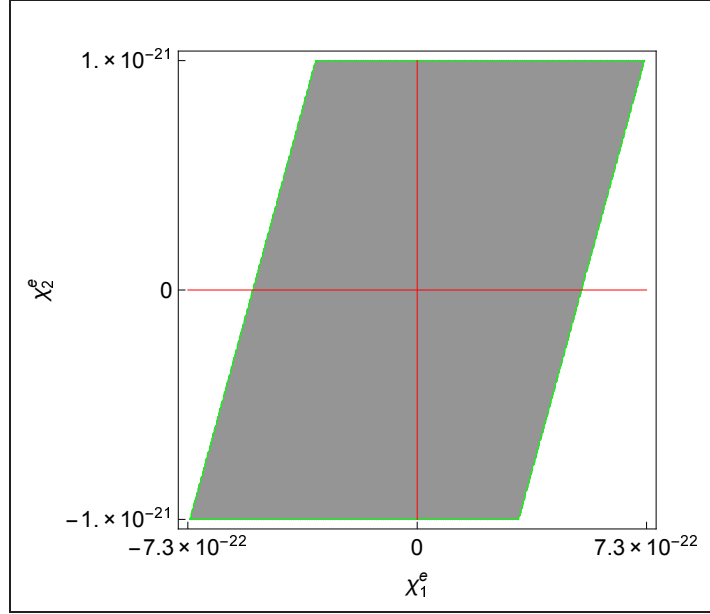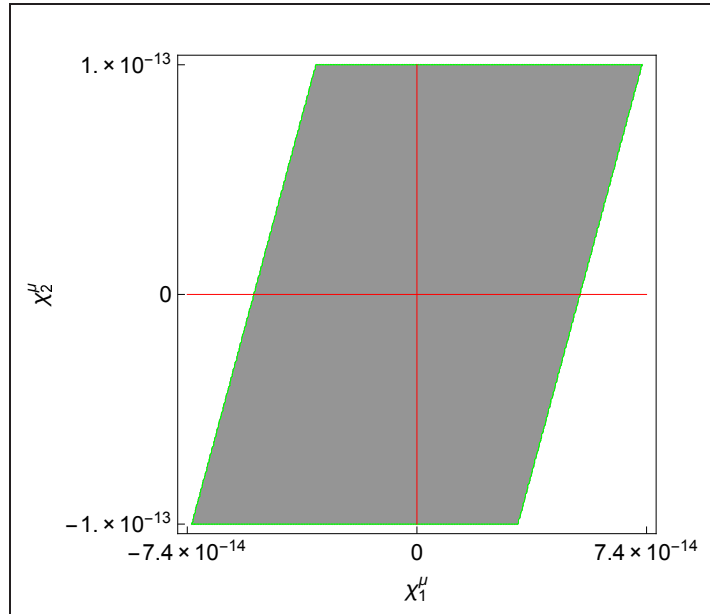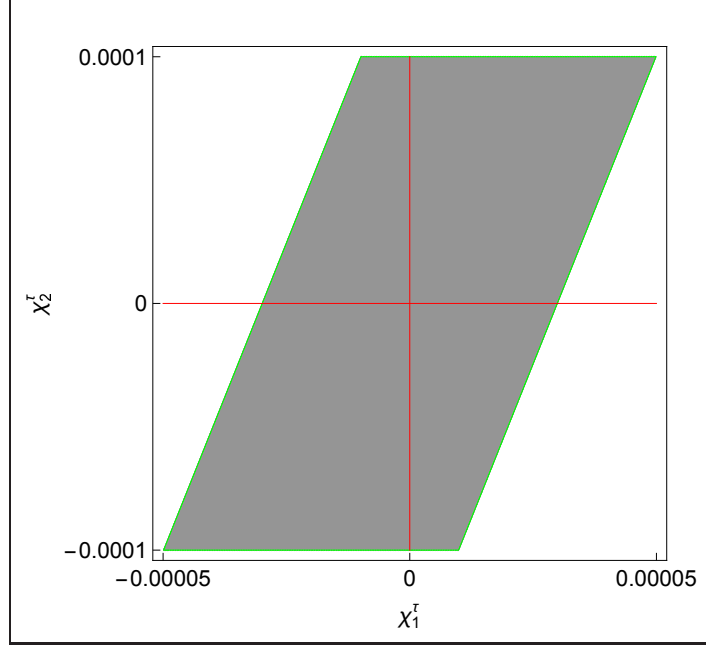
Figure 3.5: The allowed region within the parameter space $(\chi_1^\tau, \chi_2^\tau)$, for quasidegenerate texture, for $|\chi_1^\tau| < 0.5 \times 10^{-4}$ and $|\chi_2^\tau| < 10^{-4}$. We have denoted $\chi_1^{\tau\tau} = \chi_1^\tau$

maximum (top) values of χ_2^{AA} with $A = e, \mu, \tau$, as shown in Figs. (3.3)-(3.5). The same rows include the medium values of χ_1^{AA} intervals within the graphs' allowed regions, which are determined by the fixed upper and lower χ_2^{AA} parameters.

	Bottom	Top
χ_2^{ee} fixed	-1×10^{-21}	$+1 \times 10^{-21}$
$\Rightarrow \chi_1^{ee}$	-2.01×10^{-22}	$+2.01 \times 10^{-22}$
$\chi_2^{\mu\mu}$ fixed	-1×10^{-13}	$+1 \times 10^{-13}$
$\Rightarrow \chi_1^{\mu\mu}$	-2.12×10^{-14}	$+2.12 \times 10^{-14}$
$\chi_2^{\tau\tau}$ fixed	-1×10^{-4}	$+1 \times 10^{-4}$
$\Rightarrow \chi_1^{\tau\tau}$	-1.96×10^{-5}	$+1.96 \times 10^{-5}$

Table 3.6: Values of Lorentz-violation parameters χ_1^{AA} and χ_2^{AA}, with $A = e, \mu, \tau$, from lepton AMMs constraints

The determination of the bounds in the case of lepton EDMs is simpler. From Eq. (3.16), each new physics contribution to $d_{l_A}^{\text{SME}}$ is expressed in terms of only one trace. From the current limits on lepton EDMs displayed in Eqs. (3.5)-(3.8) we get

$$|d_3^{AA}\chi_3^{AA}| < |d_{l_A}|. \tag{3.18}$$

Using Eq. (3.18), the following bounds from Lorentz violating parameters are derived

$$|\chi_3^{ee}| < 5.58 \times 10^{-27}, \tag{3.19}$$

$$|\chi_3^{\mu\mu}| < 1.02 \times 10^{-10}, \tag{3.20}$$

$$-5.95 \times 10^{-5} < -i\chi_3^{\tau\tau} < 1.21 \times 10^{-4}. \tag{3.21}$$

3.2.2 Hermitian matrices $Y_{\alpha\beta}$

Consider a scenario in which $Y_{\alpha\beta}^{\dagger} = Y_{\alpha\beta}$ holds. This assumption, as previously stated, results in an exact cancellation of Lorentz violating coefficients $A_{\alpha\beta}^{AB}$ while leaving nonzero factors $V_{\alpha\beta}^{AB}$, as shown by Eqs. (1.14). Under such circumstances, only the matrix χ_1 remains nonzero, so the whole set of AMM contributions is written in terms of six χ_1 parameters, as we mention in section (3.2), whereas there are no contributions to EDMs.

To analize the AMM contributions, we define

$$\Delta_1^H = \frac{\chi_1^{e\mu}}{\chi_1^{\tau e}}, \qquad \Delta_2^H = \frac{\chi_1^{\tau e}}{\chi_1^{\mu\tau}}, \tag{3.22}$$

in terms of which the new physics contributions, shown in Eqs. (3.10), are written as

$$
\begin{aligned}
a_e^{\text{SME}} &= a_1^{ee} \chi_1^{ee} + a_1^{e\mu} \chi_1^{e\mu} + a_1^{e\tau} \chi_1^{e\tau} \\
&= a_1^{ee} \chi_1^{ee} + \frac{\chi_1^{\tau e}}{\chi_1^{\mu\tau}} \left(a_1^{e\mu} \frac{\chi_1^{e\mu}}{\chi_1^{\tau e}} + a_1^{e\tau} \right) \chi_1^{\mu\tau} \\
&= a_1^{ee} \chi_1^{ee} + \Delta_2^H \left(a_1^{e\mu} \Delta_1^H + a_1^{e\tau} \right) \chi_1^{\mu\tau},
\end{aligned} \tag{3.23}
$$

$$
\begin{aligned}
a_\mu^{\text{SME}} &= a_1^{\mu e} \chi_1^{\mu e} + a_1^{\mu\mu} \chi_1^{\mu\mu} + a_1^{\mu\tau} \chi_1^{\mu\tau} \\
&= a_1^{\mu\mu} \chi_1^{\mu\mu} + \left(a_1^{e\mu} \frac{\chi_1^{e\mu}}{\chi_1^{\tau e}} \frac{\chi_1^{\tau e}}{\chi_1^{\mu\tau}} + a_1^{\mu\tau} \right) \chi_1^{\mu\tau} \\
&= a_1^{\mu\mu} \chi_1^{\mu\mu} + \left(a_1^{e\mu} \Delta_1^H \Delta_2^H + a_1^{\mu\tau} \right) \chi_1^{\mu\tau},
\end{aligned} \tag{3.24}
$$

$$
\begin{aligned}
a_\tau^{\text{SME}} &= a_1^{\tau e} \chi_1^{\tau e} + a_1^{\tau\mu} \chi_1^{\tau\mu} + a_1^{\tau\tau} \chi_1^{\tau\tau} \\
&= a_1^{\tau\tau} \chi_1^{\tau\tau} + \left(a_1^{\tau e} \frac{\chi_1^{\tau e}}{\chi_1^{\mu\tau}} + a_1^{\tau\mu} \right) \chi_1^{\mu\tau} \\
&= a_1^{\tau\tau} \chi_1^{\tau\tau} + \left(a_1^{\tau e} \Delta_2^H + a_1^{\tau\mu} \right) \chi_1^{\mu\tau}.
\end{aligned} \tag{3.25}
$$

Each contribution to any lepton flavor A is thus expressed in terms of four parameters: for any flavor A, three such quantities are the factors Δ_1^H, Δ_2^H and the trace $\chi_1^{\mu\tau}$, while the fourth parameter χ_1^{AA} is the only one that distinguishes the specific A flavor contribution.

The fact that Eqs. (3.23) - (3.25) share three Lorentz violation parameters helps us to determine simultaneously the contributions a_e^{SME}, a_μ^{SME} and a_τ^{SME} in terms of them. The way to proceed is

assigning specific values to Δ_1^H and Δ_2^H and obtain the allowed regions in the spaces $(\chi_1^{ee}, \chi_1^{\mu\tau})$, $(\chi_1^{\mu\mu}, \chi_1^{\mu\tau})$, $(\chi_1^{\tau\tau}, \chi_1^{\mu\tau})$ for the a_e^{SME}, a_μ^{SME} and a_τ^{SME}, respectively.

The two graphs of Fig. (3.7) display the allowed regions in the space of parameters $(\chi_1^{ee}, \chi_1^{\mu\tau})$, determined by the bound on contributions from new physics to the electron AMM

$$|a_1^{ee}\chi_1^{ee} + \Delta_2^H \left(a_1^{e\mu}\Delta_1^H + a_1^{e\tau}\right)\chi_1^{\mu\tau}| < |\Delta a_e|, \tag{3.26}$$

where two scenarios were included, each with a different Δ_1^H value, in order to compare the obtained allowed regions. In one of them, the value $\Delta_1^H = 10^2$ was used, while in the other, the value $\Delta_1^H = 10^3$ was considered. Whereas for each graph the values $\Delta_2^H = 0.1, 0.2, 0.3$ have been taken into account.

We can say something about the graphs shown in Fig. (3.7)

- These graphs show how, in general, the orientations of allowed regions differ for different values of Δ_2^H with fixed Δ_1^H.

- Each graph depicts three allowed regions, which are straight strips with similar widths for each considered Δ_2^H. In the case of $\Delta_1^H = 10^2$, the allowed regions are practically indistinguishable from one another, whereas the shapes of the regions appear to be more sensitive to changes in Δ_2^H as long as $\Delta_1^H = 10^3$ is present.

The last statement realized for specific choices of factors Δ_1^H and Δ_2^H should not be interpreted to be valid in general. To demonstrate this, we present Fig. (3.8) which was realized within the same parameter region $(\chi_1^{ee}, \chi_1^{\mu\tau})$ as that of the graphs of Fig. (3.7). In this case, the values $\Delta_2^H = 1$ and $\Delta_1^H = 15, 150, 1500$ have been chosen.

It is worth noting that the largest value of Δ_2^H considered for the graphs shown in Fig. (3.8) results in an allowed stick region that is narrower, with a clockwise rotated orientation, than the others shown in Fig. (3.7). As a result, in Fig. (3.8), $\chi_1^{\mu\tau}$ is more stringently restricted than χ_1^{ee}, as opposite to the allowed regions of Fig. (3.7).

Concerning the contributions from the SME to the AMM of the muon, in this scenario, the expression a_μ^{SME} is complex valued, so its modulus, $|a_\mu^{\text{SME}}|$ has been rather considered to compare it with the bound from new physics on the muon AMM, Eq. (3.3), which corresponds to an interval of positive values.

$$|a_1^{\mu\mu}\chi_1^{\mu\mu} + \left(a_1^{e\mu}\Delta_1^H\Delta_2^H + a_1^{\mu\tau}\right)\chi_1^{\mu\tau}| < |\Delta a_\mu| \tag{3.27}$$

The graphs in Fig. (3.9) show the allowed regions in the parameter space $(\chi_1^{\mu\mu}, \chi_1^{\mu\tau})$, obtained from Eq. (3.27). Because we are analyzing the norm $|a_\mu^{\text{SME}}|$, the obtained allowed regions are not straight

Figure 3.7: Allowed regions in the parameter space $(\chi_1^{ee}, \chi_1^{\mu\tau})$ within $|\chi_1^{ee}| < 1.7 \times 10^{-21}$ and $|\chi_1^{\mu\tau}| < 10^{-21}$. In his case the value of Δ_1^H was fixed and the value of Δ_2^H was varying.
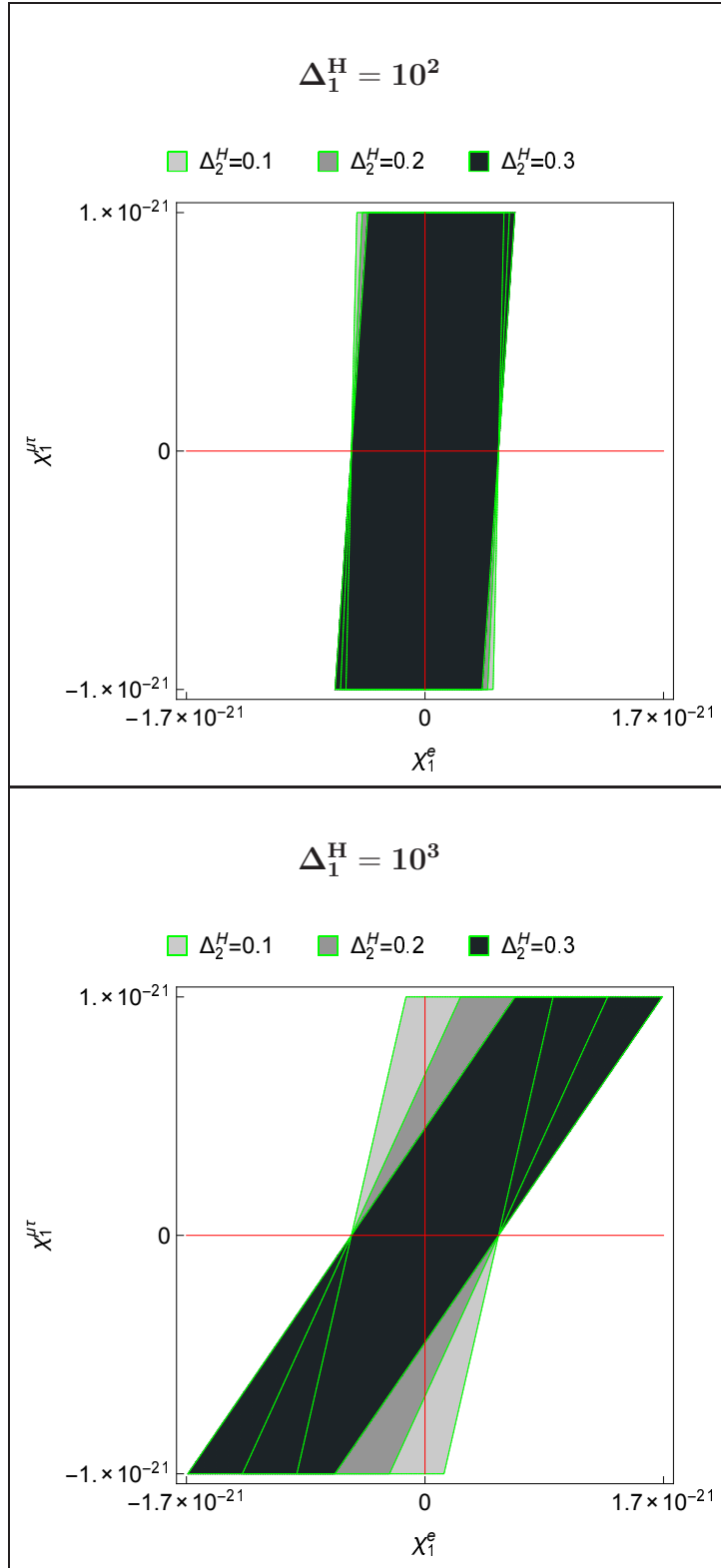
strips, but rather ovals.

Figure 3.8: Allowed regions in the parameter space $(\chi_1^{ee}, \chi_1^{\mu\tau})$ within $|\chi_1^{ee}| < 1.7 \times 10^{-21}$ and $|\chi_1^{\mu\tau}| < 10^{-21}$. In his case the value of Δ_2^H was fixed and the value of Δ_1^H was varying.

We consider values within $|\chi_1^{\mu\mu}| < 6 \times 10^{-14}$ for both graphs, whereas vertical axes range along different intervals: The upper graph vertical axis (with $\Delta_1^H = 10^2$) runs over $|\chi_1^{\mu\tau}| < 4.5 \times 10^{-15}$ the lower graph, with $\Delta_1^H = 10^3$, displays values of the vertical axis within $|\chi_1^{\mu\tau}| < 4.5 \times 10^{-16}$.

It is worth noting that, for fixed Δ_1^H, increasing the value of the parameter Δ_2^H flattens the ring along the $\chi_1^{\mu\tau}$ axis, with larger values of Δ_2^H corresponding to more restricted allowed regions. So, notice that the choice $\Delta_1^H = 10^3$ yields more constrained regions than those corresponding to $\Delta_1^H = 10^2$.

Finally, we will look at the contributions from the SME to the tau AMM. As was the case in the previous discussion of the muon case, the SME contribution a_τ^{SME} is a complex valued quantity. As a result, the modulus $|a_\tau^{\mathrm{SME}}|$ is taken into account

$$|a_1^{\tau\tau}\chi_1^{\tau\tau} + \left(a_1^{\tau e}\Delta_2^H + a_1^{\tau\mu}\right)\chi_1^{\mu\tau}| < |a_\tau^{NP}|, \tag{3.28}$$

which a_τ^{NP} is the most restrictive extreme value of the interval in the expression (3.4). Figure (3.10) serves as an illustration, it displays one sole graph plotted within $|\chi_1^{\tau\tau}| < 3.6 \times 10^{-5}$ and $|\chi_1^{\mu\tau}| < 2.2 \times 10^{-5}$. Eq. (3.28) is Δ_1^H independent, so there is no need to include additional graphs to compare regions associated with different values of the factor Δ_2^H.
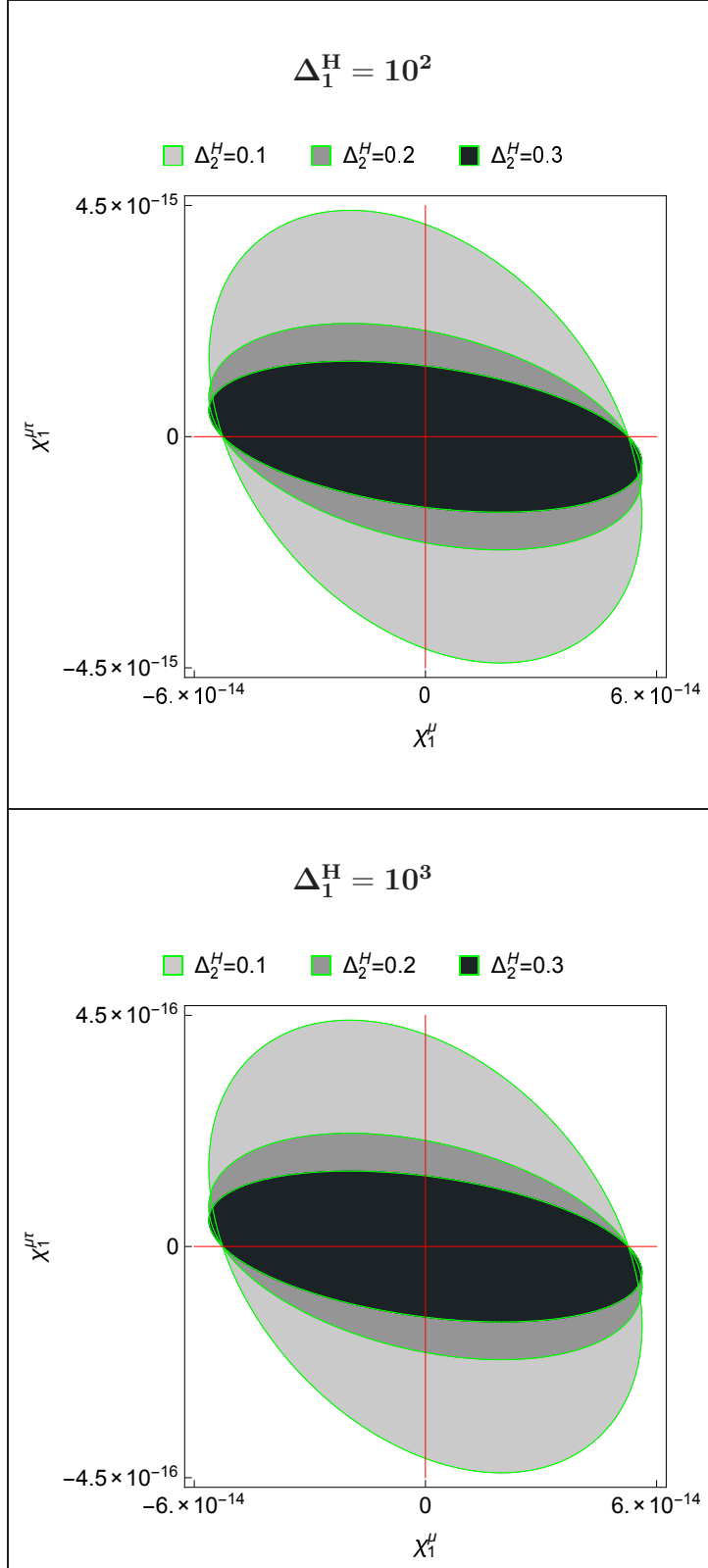
Figure 3.9: Allowed regions in the parameter space $(\chi_1^{\mu\mu}, \chi_1^{\mu\tau})$ within $|\chi_1^{\mu\mu}| < 6 \times 10^{-14}$ and $|\chi_1^{\mu\tau}| < 4.5 \times 10^{-15}$ (upper graph) or $|\chi_1^{\mu\tau}| < 4.5 \times 10^{-16}$ (lower graph). In his case the value of Δ_1^H was fixed and the value of Δ_2^H was varying.
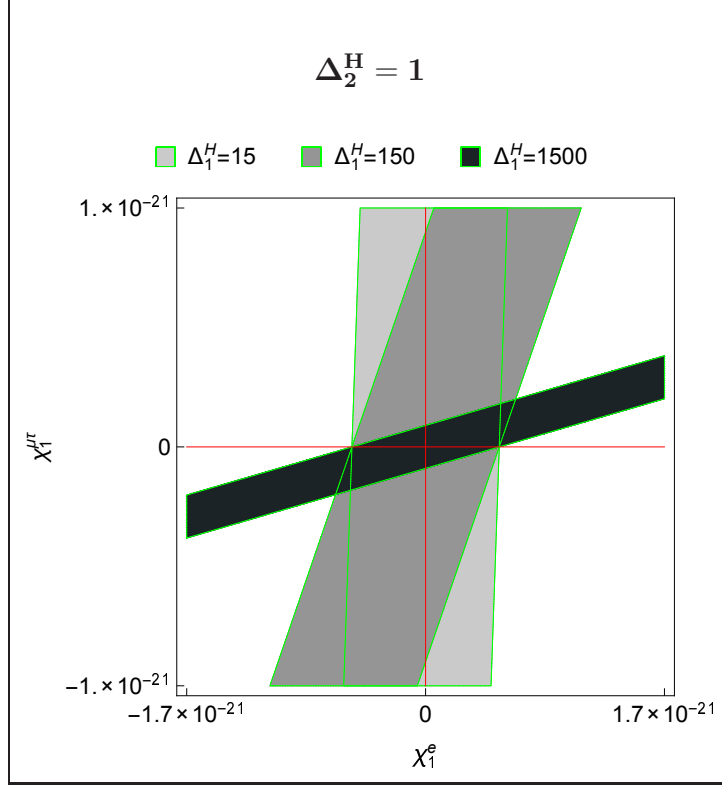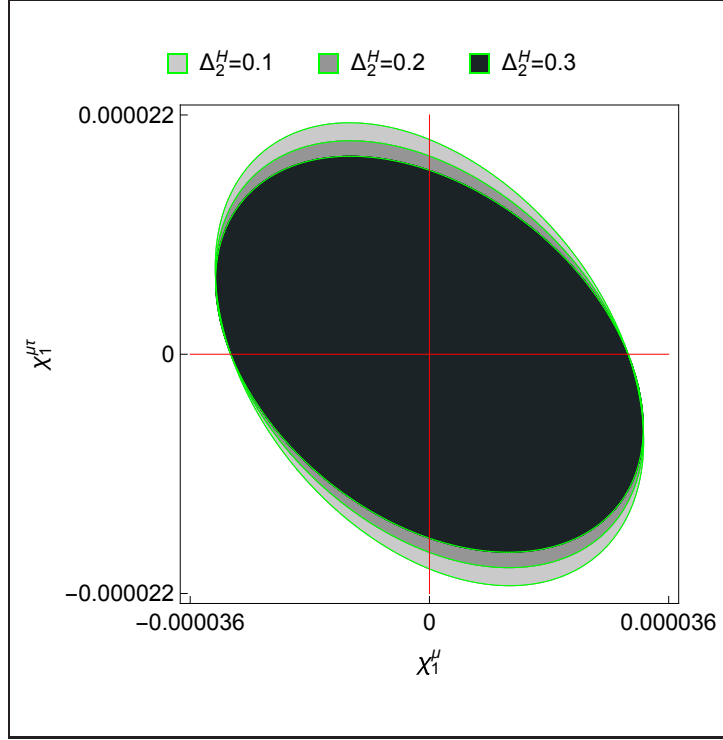
Figure 3.10: Allowed regions in the parameter space $(\chi_1^{\tau\tau}, \chi_1^{\mu\tau})$ within $|\chi_1^{\tau\tau}| < 3.6 \times 10^{-5}$ and $|\chi_1^{\mu\tau}| < 2.2 \times 10^{-5}$.

The graph (3.10)shows that the larger the value of Δ_2^H, the flatter the ellipse along the $\chi_1^{\mu\tau}$ axis and, as a result, the smaller the allowed region in the parameter space $(\chi_1^{\tau\tau}, \chi_1^{\mu\tau})$.

Among the l_e, l_μ, l_τ mSME AMM contributions, the most stringent constraints on $\chi_1^{\mu\tau}$ are set by $|a_\mu^{\text{SME}}|$ and are of orders 10^{-16} to 10^{-15}, we can verify this information in the graphs of Fig. (3.9). The corresponding allowed intervals are represented by equidistant pairs of horizontal dashed lines from the horizontal axes. Table (3.11) shows the precise numerical values of these limits which were determined from lepton AMMs bounds on new physics effects.

a_μ^{SME}		
Δ_1^H	Δ_2^H	$|\chi_1^{\mu\tau}| <$
10^2	0.1	4.5×10^{-15}
10^2	0.2	2.3×10^{-15}
10^2	0.3	1.5×10^{-15}
10^3	0.1	4.5×10^{-16}
10^3	0.2	2.2×10^{-16}
10^3	0.3	1.5×10^{-16}

Table 3.11: The most stringent allowed intervals of $\chi_1^{\mu\tau}$ values for different choices of parameters Δ_1^H and Δ_1^H. They were obtained from Fig. (3.9) in the scenario of Hermitian matrices $Y_{\alpha\beta}$.

Chapter 4

Lorentz violation in nucleon electromagnetic moments

The theory and calculations presented in the preceding chapters of this thesis can be used to analyze the EMMs of quarks, which can then be used to define contributions to the EMMs of nucleons.

In this section, we will concentrate on the renormalizable extension of the quark Yukawa sector that induces LFV via the Higgs boson, which originates in Eq. (1.10)

$$\mathcal{L}_{\text{Yukawa},q}^{\text{SME}} = -\frac{1}{2}(H_U)_{\mu\nu}^{AB}\bar{Q}_A\phi^c\sigma^{\mu\nu}U_B - \frac{1}{2}(H_D)_{\mu\nu}^{AB}\bar{Q}_A\phi\sigma^{\mu\nu}D_B + \text{h.c.}. \tag{4.1}$$

After spontaneous electroweak symmetry breaking, then yields

$$\mathcal{L}_{\text{Yukawa},q}^{\text{SME}} = -\frac{1}{2}(v+H)\sum_{f=u,d}\overline{f_A}\Big[(Y_f)_{\mu\nu}^{AB}P_L + (Y_f)_{\mu\nu}^{BA*}P_R\Big]\sigma^{\mu\nu}f_B. \tag{4.2}$$

Note that quark flavor indices A, B in Eq. (4.2) run over either u, c, t or d, s, b, depending on whether $f = u$ or $f = d$.

The dominant diagrams are the same as in the lepton case (see Fig. 2.3), but we must consider interaction with quarks rather than leptons.

Taking advantage of the property $Y_{\alpha\beta}^{AB} = -Y_{\beta\alpha}^{AB}$, we define the complex electric-like vector $Y_{0i}^{AB} = e_i^{AB}$ and the complex magnetic-like vector $Y_{ij}^{AB} = \varepsilon_{ijk}b^{AB\,k}$, drawing inspiration from the relationship between electric and magnetic fields and the corresponding electromagnetic strength tensor $F_{\mu\nu}$.

Using our calculation of the SME Yukawa sector contributions to quark electromagnetic form factors, as identified from Eq.(2.16), we write the corresponding contributions to AMMs and EDMs as

$$
\begin{aligned}
a_A^{\mathrm{SME}} &= \sum_B \left[\tilde{a}_{AB} \left(|\mathrm{Re}\,\mathbf{e}^{AB}|^2 + |\mathrm{Re}\,\mathbf{b}^{AB}|^2 \right) \right. \\
&\qquad \left. + \hat{a}_{AB} \left(|\mathrm{Im}\,\mathbf{e}^{AB}|^2 + |\mathrm{Im}\,\mathbf{b}^{AB}|^2 \right) \right],
\end{aligned}
\tag{4.3}
$$

$$
d_A^{\mathrm{SME}} = \sum_B \tilde{d}_{AB} \left(|\mathrm{Re}\,\mathbf{e}^{AB}| |\mathrm{Im}\,\mathbf{b}^{AB}| + |\mathrm{Re}\,\mathbf{b}^{AB}| |\mathrm{Im}\,\mathbf{e}^{AB}| \right).
\tag{4.4}
$$

Because these electromagnetic contributions are entirely given by real and imaginary parts of Lorentz violation coefficients $\mathbf{e}^{AB}$ and $\mathbf{b}^{AB}$, these are the quantities to be compared with experimental results and thus to bound, remembering that the original SME coefficients that comprise them are $(H_u)_{\mu\nu}^{AB}$ and $(H_d)_{\mu\nu}^{AB}$, as introduced in Eq. (4.1).

It is important to mention that we find UV finite results, thought IR divergences remain. As we argued previously, such divergences are expected to disappear from cross sections, so we will ignore them for the remainder of our discussion. It should be noted, however, that AMMs and EDMs are not observables, despite the fact that they can provide estimates of the impact of Lorentz violation on physical processes involving the quark electromagnetic vertex.

4.1 EMMs of nucleons

To constrain Lorentz violation coefficients, we consider EMMs of nucleons. The Particle Data Group recommends the following nucleon AMM values [130]:

- $\mu_p = 2.7928473446(8)\mu_N$ [131], for the proton.

- $\mu_n = -1.9130427(5)\mu_N$ [132], for the neutron.

The nuclear magneton is denoted by μ_N in both expressions. Assuming that new physics could be as large as the errors in these data, we chose the proton magnetic moment measurement to constrain SME coefficients because its error is three orders of magnitude smaller than that of the neutron.

In terms of EDMs, the Particle Data Group leans towards

- $|d_p| < 2.1 \times 10^{-25} e\,\mathrm{cm}$ [133], for the proton.

- $|d_n| < 1.8 \times 10^{-26} e\,\mathrm{cm}$ [134], in the case of the neutron.

We use the neutron bound to constrain SME parameters.

Using standard prescriptions, we connect these nucleon EMMs to those of constituent quarks.

$$
a_p = \frac{4}{3} a_u - \frac{1}{3} a_d,
\tag{4.5}
$$

$$d_n = \frac{4}{3}d_d - \frac{1}{3}d_u. \tag{4.6}$$

obtaining

$$a_p^{\text{SME}} = \sum_B \frac{4}{3} \left[\tilde{a}_{uB} \left(|\text{Re}\,\mathbf{e}^{uB}|^2 + |\text{Re}\,\mathbf{b}^{uB}|^2 \right) + \hat{a}_B \left(|\text{Im}\,\mathbf{e}^{uB}|^2 + |\text{Im}\,\mathbf{b}^{uB}|^2 \right) \right]$$

$$- \sum_B \frac{1}{3} \left[\tilde{a}_{dB} \left(|\text{Re}\,\mathbf{e}^{dB}|^2 + |\text{Re}\,\mathbf{b}^{dB}|^2 \right) + \hat{a}_B \left(|\text{Im}\,\mathbf{e}^{dB}|^2 + |\text{Im}\,\mathbf{b}^{dB}|^2 \right) \right]. \tag{4.7}$$

$$d_n^{\text{SME}} = - \sum_B \frac{1}{3} \tilde{d}_{uB} \left(|\text{Re}\,\mathbf{e}^{uB}||\text{Im}\,\mathbf{b}^{uB}| + |\text{Re}\,\mathbf{b}^{uB}||\text{Im}\,\mathbf{e}^{uB}| \right)$$

$$+ \sum_B \frac{4}{3} \tilde{d}_{dB} \left(|\text{Re}\,\mathbf{e}^{dB}||\text{Im}\,\mathbf{b}^{dB}| + |\text{Re}\,\mathbf{b}^{dB}||\text{Im}\,\mathbf{e}^{dB}| \right) \tag{4.8}$$

Table 4.1 displays upper bounds on maximal attained sensitivities of the real and imaginary parts of $\mathbf{e}^{AB}$ and $\mathbf{b}^{AB}$ derived from our expression for the SME Yukawa sector contribution to the proton AMM.

LVP	Bounds
$|\text{Re}\{\mathbf{e}^{uu}, \mathbf{b}^{uu}\}|$	9.028×10^{-10}
$|\text{Im}\{\mathbf{e}^{uu}, \mathbf{b}^{uu}\}|$	2.019×10^{-9}
$|\text{Re}\{\mathbf{e}^{uc}, \mathbf{b}^{uc}\}|$	2.541×10^{-8}
$|\text{Im}\{\mathbf{e}^{uc}, \mathbf{b}^{uc}\}|$	2.546×10^{-8}
$|\text{Re}\{\mathbf{e}^{ut}, \mathbf{b}^{ut}\}|$	9.461×10^{-11}
$|\text{Im}\{\mathbf{e}^{ut}, \mathbf{b}^{ut}\}|$	9.461×10^{-11}
$|\text{Re}\{\mathbf{e}^{dd}, \mathbf{b}^{dd}\}|$	9.028×10^{-9}
$|\text{Im}\{\mathbf{e}^{dd}, \mathbf{b}^{dd}\}|$	2.019×10^{-8}
$|\text{Re}\{\mathbf{e}^{ds}, \mathbf{b}^{ds}\}|$	4.320×10^{-8}
$|\text{Im}\{\mathbf{e}^{ds}, \mathbf{b}^{ds}\}|$	4.550×10^{-8}
$|\text{Re}\{\mathbf{e}^{db}, \mathbf{b}^{db}\}|$	2.901×10^{-7}
$|\text{Im}\{\mathbf{e}^{db}, \mathbf{b}^{db}\}|$	2.936×10^{-7}

Table 4.1: Bounds from the proton AMM on Lorentz violation parameters (LVP) of the minimal SME Yukawa sector. $\text{Re}\{\mathbf{e}^{AB}, \mathbf{b}^{AB}\}$ denotes both $\text{Re}\,\mathbf{e}^{AB}$ and $\text{Re}\,\mathbf{b}^{AB}$, and the same applies for imaginary parts.

The bounds from the neutron EDM, were calculated in two different ways.

- Consider some fixed quark flavor index u, B or d, B, in the sum defining the EDM contribution in Eq. (4.8) and assume that all contributions associated with other index combinations vanish. The remainder of the terms were then bound using experimental data. Table (4.2) displays the resulting constraints for each fixed u, B or d, B. It is an illustrative method of comparing sensitivities to SME coefficients of experiments measuring proton AMMs with those aimed at neutron EDMs.

- In the alternative scenario, assume that all SME parameters $|\mathrm{Re}\,\mathbf{e}^{AB}|$, $|\mathrm{Re}\,\mathbf{b}^{AB}|$, $|\mathrm{Im}\,\mathbf{e}^{AB}|$, and $|\mathrm{Im}\,\mathbf{b}^{AB}|$ are nearly equal. Table (4.3) shows the experimental bound for neutron EDM in such circumstances.

In this section, we calculated the contributions to the EMMs of quarks from the renormalizable SME Yukawa sector, using the standard prescription for connecting quark EMMs to nucleon EMMs. Our findings were used to estimate proton and neutron contributions to AMMs and EDMs, which were then compared to current bounds to yield constraints on SME coefficients that parametrize the effects of Lorentz violation at low energies. Bounds as stringent as 10^{-12} have been established.

EMM	Bounds	Best
a_p	$\left\vert 1.963\vert\operatorname{Re}\mathbf{e}^{uu}\vert^2 + 0.393\vert\operatorname{Im}\mathbf{b}^{uu}\vert^2\right\vert < 1.6\times 10^{-18}$	
d_n	$0.970\vert\operatorname{Re}\mathbf{e}^{uu}\vert\vert\operatorname{Im}\mathbf{b}^{uu}\vert < 1.8\times 10^{-23}$	✓
a_p	$\left\vert 1.963\vert\operatorname{Re}\mathbf{b}^{uu}\vert^2 + 0.393\vert\operatorname{Im}\mathbf{e}^{uu}\vert^2\right\vert < 1.6\times 10^{-18}$	
d_n	$0.970\vert\operatorname{Re}\mathbf{b}^{uu}\vert\vert\operatorname{Im}\mathbf{e}^{uu}\vert < 1.8\times 10^{-23}$	✓
a_p	$\left\vert 2.479\vert\operatorname{Re}\mathbf{e}^{uc}\vert^2 - 2.468\vert\operatorname{Im}\mathbf{b}^{uc}\vert^2\right\vert < 1.6\times 10^{-15}$	
d_n	$2.037\vert\operatorname{Re}\mathbf{e}^{uc}\vert\vert\operatorname{Im}\mathbf{b}^{uc}\vert < 1.8\times 10^{-20}$	✓
a_p	$\left\vert 2.479\vert\operatorname{Re}\mathbf{b}^{uc}\vert^2 - 2.468\vert\operatorname{Im}\mathbf{e}^{uc}\vert^2\right\vert < 1.6\times 10^{-15}$	
d_n	$2.037\vert\operatorname{Re}\mathbf{b}^{uc}\vert\vert\operatorname{Im}\mathbf{e}^{uc}\vert < 1.8\times 10^{-20}$	✓
a_p	$\left\vert 1.787\vert\operatorname{Re}\mathbf{e}^{ut}\vert^2 + 1.787\vert\operatorname{Im}\mathbf{b}^{ut}\vert^2\right\vert < 1.6\times 10^{-20}$	✓
d_n	$1.497\vert\operatorname{Re}\mathbf{e}^{ut}\vert\vert\operatorname{Im}\mathbf{b}^{ut}\vert < 1.8\times 10^{-18}$	
a_p	$\left\vert 1.787\vert\operatorname{Re}\mathbf{b}^{ut}\vert^2 + 1.787\vert\operatorname{Im}\mathbf{e}^{ut}\vert^2\right\vert < 1.6\times 10^{-20}$	✓
d_n	$1.497\vert\operatorname{Re}\mathbf{b}^{ut}\vert\vert\operatorname{Im}\mathbf{e}^{ut}\vert < 1.8\times 10^{-18}$	
a_p	$\left\vert 1.963\vert\operatorname{Re}\mathbf{e}^{dd}\vert^2 + 0.393\vert\operatorname{Im}\mathbf{b}^{dd}\vert^2\right\vert < 1.6\times 10^{-16}$	
d_n	$6.208\vert\operatorname{Re}\mathbf{e}^{dd}\vert\vert\operatorname{Im}\mathbf{b}^{dd}\vert < 1.8\times 10^{-21}$	✓
a_p	$\left\vert 1.963\vert\operatorname{Re}\mathbf{b}^{dd}\vert^2 + 0.393\vert\operatorname{Im}\mathbf{e}^{dd}\vert^2\right\vert < 1.6\times 10^{-16}$	
d_n	$6.208\vert\operatorname{Re}\mathbf{b}^{dd}\vert\vert\operatorname{Im}\mathbf{e}^{dd}\vert < 1.8\times 10^{-21}$	✓
a_p	$\left\vert -8.575\vert\operatorname{Re}\mathbf{e}^{ds}\vert^2 + 7.727\vert\operatorname{Im}\mathbf{b}^{ds}\vert^2\right\vert < 1.6\times 10^{-14}$	
d_n	$4.329\vert\operatorname{Re}\mathbf{e}^{ds}\vert\vert\operatorname{Im}\mathbf{b}^{ds}\vert < 1.8\times 10^{-20}$	✓
a_p	$\left\vert -8.575\vert\operatorname{Re}\mathbf{b}^{ds}\vert^2 + 7.727\vert\operatorname{Im}\mathbf{e}^{ds}\vert^2\right\vert < 1.6\times 10^{-14}$	
d_n	$4.329\vert\operatorname{Re}\mathbf{b}^{ds}\vert\vert\operatorname{Im}\mathbf{e}^{ds}\vert < 1.8\times 10^{-20}$	✓
a_p	$\left\vert -1.901\vert\operatorname{Re}\mathbf{e}^{db}\vert^2 + 1.857\vert\operatorname{Im}\mathbf{b}^{db}\vert^2\right\vert < 1.6\times 10^{-13}$	
d_n	$0.990\vert\operatorname{Re}\mathbf{e}^{db}\vert\vert\operatorname{Im}\mathbf{b}^{db}\vert < 1.8\times 10^{-19}$	✓
a_p	$\left\vert -1.901\vert\operatorname{Re}\mathbf{b}^{db}\vert^2 + 1.857\vert\operatorname{Im}\mathbf{e}^{db}\vert^2\right\vert < 1.6\times 10^{-13}$	
d_n	$0.990\vert\operatorname{Re}\mathbf{b}^{db}\vert\vert\operatorname{Im}\mathbf{e}^{db}\vert < 1.8\times 10^{-19}$	✓

Table 4.2: Comparison of sensitivities to SME coefficients of experimental bounds from the proton AMM and the neutron EDM.

LVP	Bounds
$\vert\mathbf{e}^{uu}, \mathbf{b}^{uu}\vert$	4.308×10^{-12}
$\vert\mathbf{e}^{uc}, \mathbf{b}^{uc}\vert$	9.401×10^{-11}
$\vert\mathbf{e}^{ut}, \mathbf{b}^{ut}\vert$	1.096×10^{-9}
$\vert\mathbf{e}^{dd}, \mathbf{b}^{dd}\vert$	1.703×10^{-11}
$\vert\mathbf{e}^{ds}, \mathbf{b}^{ds}\vert$	6.449×10^{-11}
$\vert\mathbf{e}^{db}, \mathbf{b}^{db}\vert$	4.264×10^{-10}

Table 4.3:   Bounds from the neutron EDM on LVPs of the minimal SME Yukawa sector. $\vert\mathbf{e}^{AB}, \mathbf{b}^{AB}\vert$ denotes both $\vert\mathbf{e}^{AB}\vert$ and $\vert\mathbf{b}^{AB}\vert$.

Chapter 5

Conclusions

The present investigation was carried out in the context established by the Lorentz and CPT violating Standard Model Extension, an effective field theory that establishes a very general framework for quantifying the effects to be expected from a higher energy formulation incorporating Lorentz invariance violation at relatively low energies.

In a perturbative approach, the Lorentz violating interactions generated by the extended Yukawa sector, after implementation of the Higgs mechanism, yield two point insertions and three point vertices that induce one loop corrections to the electromagnetic vertex $A_\mu l_A l_A$. The loop corrections involve contributions to both magnetic and electric form factors. These quantities are consistently Lorentz invariant, the contributions from this new physics emerge for the first time at the second order in Lorentz-violating coefficients. We identified the leading contributions from Lorentz violation to anomalous magnetic moments, in terms of $\mathrm{tr}\kappa_1^{AB}$ and $\mathrm{tr}\kappa_2^{AB}$, and electric dipole moments, in terms of $\mathrm{tr}\kappa_2^{AB}$.

Lorentz violation results in ultraviolet finite contributions to anomalous magnetic moments and electric dipole moments. Despite this, the contributions contain infrared divergences which have been removed from the contributions to estimate the impact of these interactions on some physical process.

To constrain the Lorentz violating parameters, coming from lepton EMMs, we investigated two scenarios:

quasidiagonal textures scenario, in which all contributions from Lorentz violation are real. The electron EDM establishes the most stringent bounds restricting SME coefficients $\mathrm{tr}\kappa_j^{ee}$ at the order 10^{-27}, whereas AMMs limits on new physics effects are of order 10^{-22}. The restrictions on the tau lepton EMM bounds determine the weakest constraints for both electromagnetic moment Lorentz violation contributions, as expected.

Hermitian Yukawa matrices scenario, here no contributions to electric dipole moments are

generated, the Lorentz violation contributions to the anomalous magnetic moments of the muon and the tau lepton, which are unstable particles, have turned out to be complex quantities. The parameter $|\text{tr}\kappa_1^{\mu\tau}|$ is the one which has been bounded, its most restrictive limit is as stringent as 10^{-16}.

A summary of the bounds determined in both scenarios is provided in Table (5.1), where "QDT" and "HYM" are the acronyms for quasidiagonal textures and Hermitian Yukawa matrices, respectively. The table (5.2) displays the maximum attained sensitivities for the AMMs and EDMs of leptons.

Assumptions	EMMs	Combinations	Bounds
QDT, $|\text{tr}\,\kappa_2^{ee}| < 10^{-21}$	a_e^{SME}	$|\text{tr}\,\kappa_1^{ee}|$	$< 7.24 \times 10^{-22}$
QDT, $|\text{tr}\,\kappa_2^{\mu\mu}| < 10^{-13}$	a_μ^{SME}	$|\text{tr}\,\kappa_1^{\mu\mu}|$	$< 7.26 \times 10^{-14}$
QDT, $|\text{tr}\,\kappa_2^{\tau\tau}| < 10^{-4}$	a_τ^{SME}	$|\text{tr}\,\kappa_1^{\tau\tau}|$	$< 4.98 \times 10^{-5}$
QDT	d_e^{SME}	$|\text{tr}\,\kappa_3^{ee}|$	$< 5.58 \times 10^{-27}$
QDT	d_μ^{SME}	$|\text{tr}\,\kappa_3^{\mu\mu}|$	$< 1.02 \times 10^{-10}$
QDT	d_τ^{SME}	$-i\,\text{tr}\,\kappa_3^{ee}$	$> -5.95 \times 10^{-5}$
			$< 1.21 \times 10^{-4}$
HYM, $\Delta_1^{\text{H}} = 10^2$, $\Delta_2^{\text{H}} = 0.3$	$|a_\mu^{\text{SME}}|$	$|\text{tr}\,\kappa_1^{\mu\tau}|$	$< 1.44 \times 10^{-15}$
HYM, $\Delta_1^{\text{H}} = 10^3$, $\Delta_2^{\text{H}} = 0.3$	$|a_\mu^{\text{SME}}|$	$|\text{tr}\,\kappa_1^{\mu\tau}|$	$< 1.45 \times 10^{-16}$

Table 5.1: Most restrictive bounds on SME coefficients from the Lorentz violating Yukawa sector.

After calculating the AMM of the proton, we get the most stringent limit, of order $\sim 10^{-11}$, which is established on the SME parameters $\mathbf{e}^{ut}$ and $\mathbf{b}^{ut}$, linking the physics of Lorentz invariance violation of the u and t quarks. The best constraint provided by the neutron EDM is for the quark flavors $f = u$, $B = t$, of the order of $\sim 10^{-20}$; this is the only case in which the proton AMM yields the most stringent limit. With the second analysis, $|\mathbf{e}^{uu}|$ and $|\mathbf{b}|^{uu}$ are limited to values as small as 10^{-12}.

EMMs	Parameters	Upper bounds
a_e^{SME}	$\lvert\operatorname{tr}\kappa_1^{ee}\rvert$	5.24×10^{-22}
	$\lvert\operatorname{tr}\kappa_1^{e\mu}\rvert$	1.35×10^{-19}
	$\lvert\operatorname{tr}\kappa_1^{e\tau}\rvert$	2.28×10^{-18}
	$\lvert\operatorname{tr}\kappa_2^{ee}\rvert$	2.62×10^{-21}
	$\lvert\operatorname{tr}\kappa_2^{e\mu}\rvert$	1.36×10^{-19}
	$\lvert\operatorname{tr}\kappa_2^{e\tau}\rvert$	2.28×10^{-18}
a_μ^{SME}	$\lvert\operatorname{tr}\kappa_1^{\mu e}\rvert$	4.12×10^{-14}
	$\lvert\operatorname{tr}\kappa_1^{\mu\mu}\rvert$	5.26×10^{-14}
	$\lvert\operatorname{tr}\kappa_1^{\mu\tau}\rvert$	1.05×10^{-12}
	$\lvert\operatorname{tr}\kappa_2^{\mu e}\rvert$	4.21×10^{-14}
	$\lvert\operatorname{tr}\kappa_2^{\mu\mu}\rvert$	2.63×10^{-13}
	$\lvert\operatorname{tr}\kappa_2^{\mu\tau}\rvert$	1.18×10^{-12}
a_τ^{SME}	$\lvert\operatorname{tr}\kappa_1^{\tau e}\rvert$	2.36×10^{-5}
	$\lvert\operatorname{tr}\kappa_1^{\tau\mu}\rvert$	2.15×10^{-5}
	$\lvert\operatorname{tr}\kappa_1^{\tau\tau}\rvert$	2.99×10^{-5}
	$\lvert\operatorname{tr}\kappa_2^{\tau e}\rvert$	2.37×10^{-5}
	$\lvert\operatorname{tr}\kappa_2^{\tau\mu}\rvert$	2.64×10^{-5}
	$\lvert\operatorname{tr}\kappa_2^{\tau\tau}\rvert$	1.49×10^{-4}
d_e^{SME}	$\lvert\operatorname{tr}\kappa_3^{ee}\rvert$	1.12×10^{-26}
	$\lvert\operatorname{tr}\kappa_3^{e\mu}\rvert$	8.65×10^{-25}
	$\lvert\operatorname{tr}\kappa_3^{e\tau}\rvert$	1.46×10^{-23}
d_μ^{SME}	$\lvert\operatorname{tr}\kappa_3^{\mu e}\rvert$	6.09×10^{-5}
	$\lvert\operatorname{tr}\kappa_3^{\mu\mu}\rvert$	1.02×10^{-10}
	$\lvert\operatorname{tr}\kappa_3^{\mu\tau}\rvert$	1.28×10^{-9}
d_τ^{SME}	$\lvert\operatorname{tr}\kappa_3^{\tau e}\rvert$	1.19×10^{5}
	$\lvert\operatorname{tr}\kappa_3^{\tau\mu}\rvert$	3.47×10^{-2}
	$\lvert\operatorname{tr}\kappa_3^{\tau\tau}\rvert$	6.31×10^{-5}

Table 5.2: Most restrictive bounds on SME coefficients from the Lorentz violating Yukawa sector.

Bibliography

[1] A. Einstein, Ann. Phys. **17**, 891 (1905).

[2] E. P. Wigner, Ann. Math. **40**, 149 (1939).

[3] S. Weinberg, The quantum theory of fields, Cambridge University Press, 1995.

[4] A. Einstein, Math. Phys., pp 778 (1915).

[5] A. Einstein, Math. Phys., pp 778 (1944).

[6] V. A. Kostelecký, Gravity, Phys. Rev. D **69**, 105009 (2004).

[7] D. Colladay, V. A. Kostelecky, Phys. Rev. D **58**, 116002 (1998).

[8] M. Tanabashi, et al. (Particle Data Group), Phys. Rev. D **98**, 030001 (2018).

[9] P. J. Mohr, B. N. Taylor, and D. B. Newell, Rev. Mod. Phys. **80**, 633 (2008).

[10] V. A. Kostelecký and R. Potting, Nucl. Phys. B **359**, 545 (1991).

[11] V. A. Kostelecký and S. Samuel, Phys. Rev. D **39**, 683 (1989).

[12] S. M. Carroll, J. A. Harvey, V. A. Kostelecký, C. D. Lane, and T. Okamoto, Phys. Rev. Lett. **87**, 141601 (2001)

[13] V. A. Kostelecký and R. Potting, Phys. Rev. D **51**, 3923 (1995).

[14] S. M. Carroll, J. A. Harvey, V. A. Kostelecký, C. D. Lane, and T. Okamoto, Phys. Rev. Lett. **87**, 141601 (2001).

[15] D. Mattingly, Living Rev. Rel. **8**, 5 (2005).

[16] V. A. Kostelecký and N. Russell, Rev. Mod. Phys. **83**, 11 (2011).

[17] A. Dobado, A. Gómez-Nicola, A. L. Maroto, and J. R. Peláez, Effective Lagrangians for the Standard Model, Springer Verlag, Berlin, 1997.

[18] D. Colladay and V. A. Kostelecký,Phys. Rev. D **55**, 6760 (1997).

[19] D. Colladay and V. A. Kostelecký, Phys. Rev. D **58**, 116002 (1998).

[20] V. A. Kostelecký and M. Mewes, Phys. Rev. D **66**, 056005 (2002).

[21] V. A. Kostecký and M. Mewes, Phys. Rev. D **80**, 015020 (2009).

[22] R. Lehnert and R. Potting, Phys. Rev. Lett. **93**, 110402 (2004).

[23] R. Lehnert and R. Potting, Phys. Rev. D **70**, 125010 (2004).

[24] B. Altschul, Phys. Rev. Lett. **98**, 041603 (2007).

[25] B. Altschul, Phys. Rev. D **75**, 105003 (2007).

[26] B. Altschul, Nucl. Phys. B **796**, 262 (2008).

[27] B. Altschul, Phys. Rev. D **90**, 021701 (2014).

[28] V. A. Kostecký and M. Mewes, Phys. Rev. D **70**, 031902 (2004).

[29] V. A. Kostecký and M. Mewes, Phys. Rev. D **69**, 016005 (2004).

[30] J. S. Díaz and V. A. Kostecký, Phys. Rev. D **85**, 016013 (2012).

[31] J. S. Díaz, T. Katori, J. Spitz, and J. M. Conrad, Phys. Lett. B **727**, 412 (2013).

[32] A. Moyotl, H. Novales-Sánchez, J. J. Toscano, and E. S. Tututi, Int. J. Mod. Phys. A **29**, 1450039 (2014).

[33] A. Moyotl, H. Novales-Sánchez, J. J. Toscano, and E. S. Tututi, Int. J. Mod. Phys. A **29**, 1450107 (2014).

[34] V. A. Kostecký, C. D. Lane, and A. G. M. Pickering, Phys. Rev. D **65**, 056006 (2002).

[35] J. Castro-Medina, H. Novales-Sánchez, J. J. Toscano, and E. S. Tututi, Int. J. Mod. Phys. A **30**, 1550216 (2015).

[36] V. A. Kostecký and M. Mewes, Phys. Rev. D **85**, 096005 (2012).

[37] V. A. Kostecký and M. Mewes, Phys. Rev. D **88**, 096006 (2013).

[38] T. Mariz, J. R. Nascimento, A. Yu Petrov, and H. Belich, J. Phys. Commun. **1**, 045011 (2017).

[39] R. Casaca, M. M. Ferreira, L. Lisboa-Santos, F. E. P. dos Santos, and M. Schreck, Phys. Rev. D **97**, 115043 (2018).

[40] M. M. Ferreira, L. Lisboa, R. V. Maluf, and M. Schreck, Phys. Rev. D **100**, 055036 (2019).

[41] R. Potting, Journal of physics: Conference Series, **447**, 012009 (2013).

[42] A. Connes and D. Kreimer, Commun. Math. Phys. **199,** 203 (1998).

[43] V. A. Kostecký and C. Samuel, Phys. Rev. D **39**, 683 (1989).

[44] R. Gambini and J. Pullin, Phys. Rev. D **59**, 124021 (1999).

[45] R. Bluhm and V. A. Kostecký, Phys. Rev. D **71**, 065008 (2005).

[46] P. Kraus and E. T. Tomboulis, Phys. Rev. D **66**, 045015 (2002).

[47] V. A. Kostelecký and R. Potting, Gen. Rel. Grav. **37**, 1675 (2005); V. A. Kostelecký and R. Potting, Phys. Rev. D **79**, 065018 (2009).

[48] J. Schwinger, Proc. Nat. Acad. Sci. **37**, 452 (1951).

[49] O. W. Greenberg, Phys. Rev. Lett. **89**, 231602 (2002).

[50] B. R. Heckel, E. G. Adelberger, C. E. Cramer, T. S. Cook, S. Schlamminger, and U. Schmidt Phys. Rev. D **78**, 092006 (2008).

[51] H. Dehmelt, R. Mittleman, R. S. Van Dyck, and P. Schwinberg, Phys. Rev. Lett. **83**, 4694 (1999).

[52] C. Gemmel, W. Heil, S. Karpuk, K. Lenz, Yu. Sobolev, K. Tullney, M. Burghoff, W. Kilian, S. Knappe-Grüneberg, W. Müller, A. Schnabel, F. Seifert, L. Trahms, and U. Schmidt, Phys. Rev. D **82**, 111901 (2010).

[53] D. Colladay and V. A. Kostelecky, Phys. Rev. D **55** 6760 (1997).

[54] V.A. Kostelecky, Proceedings of the 4th Meeting On CPT and Lorentz Symmetry, p. 50-56 (2007).

[55] D. Mattingly, Living Rev. Relativ. **8**, 5 (2005).

[56] A. A. Michelson, E. W. Morley, American Journal of Science, issue 203, pp. 333-345 (1887).

[57] J. R Kennedy and E. M. Thorndike, Phys. Rev. **42**, 400 (1932).

[58] J. A. Lipa, J. A. Nissen, S. Wang, D. A. Stricker, and D. Avaloff, Phys. Rev. Lett. **90**, 060403 (2003).

[59] M. Nagel, S. Parker, E. Kovalchuk, Nat Commun. **6**, 8174 (2015).

[60] P. Wolf, M. E. Tobar, S. Bize, General Relativity and Gravitation **36**, 2351–2372 (2004).

[61] L. S. Brown, and G. Gabrielse, Rev. Mod. Phys. **58**, 233 (1986).

[62] D. Bear, R. E. Stoner, R. L. Walsworth, V. A. Kostelecký, and C. d. Lane, Phys. Rev. Lett. **85**, 5038 (2000)

[63] D. Bear, R. E. Stoner, R. L. Walsworth, V. A. Kostelecký, and C. d. Lane, Phys. Rev. Lett. **89**, 209902 (2002).

[64] B. R. Heckel, E. G. Adelberger, C. E. Cramer, T. S. Cook, S. Schlamminger, and U. Schmidt, Phys. Rev. D **78**, 092006 (2008).

[65] V. W. Hughes, Phys. Rev. Lett. **87**, 111804 (2001).

[66] R. Bluhm, V. A. Kostelecký, and C. D. Lane, Phys. Rev. Lett. **84**, 1098–1101 (2000).

[67] J. Bailey, et al. (CERN-Mainz-Daresbury), Nucl. Phys. B, **150**, 1 (1979).

[68] R. M. Carey, et al., Phys. Rev. Lett. **82**, 1632 (1999).

[69] D. L. Anderson, M. Sher, and I. Turan, Phys. Rev. D **70**, 016001 (2004).

[70] M. Sean, G. B. Field, and R. Jackiw, Phys. Rev. D **41**, 1231 (1990).

[71] V. A. Kostelecký and M. Mewes, Phys. Rev. Lett. **87**, 251304 (2001).

[72] D. Götz, P. Laurent, S. Antier, S. Covino, P. D'Avanzo, V. D'Elia, A. Melandri, Monthly Notices of the Royal Astronomical Society, Volume 444, Issue 3, (2014).

[73] L. Maccione, S. Liberati, A. Celotti, J. G. Kirk, and P. Ubertini, Phys. Rev. D **78**, 103003 (2008).

[74] T. Jacobson, S. Liberati, and D. Mattingly, Phys. Rev. D, **67**, 124011 (2003).

[75] V. Baccetti, K. Tate, and M. Visser, Journal of High Energy Physics, **3**, 87 (2012).

[76] C. Heinicke, P. Baekler, and F. W. Hehl, Phys. Rev. D **72**, 025012 (2015).

[77] R. Hellings, and K. Nordvedt, Phys. Rev. D **7**, 3593 (1973).

[78] D. Heyman, F. Hinteleitner, and S. Major, Phys. Rev. D **69**, 105016 (2004).

[79] I. Hinchliffe and N. Kersting, Int. J. Mod. Phys. A **19**, 204 (2004).

[80] L. Maccione, S. Liberati, A. Celotti, and J. G. Kirk, J. Cosmology Astropart. Phys. **10**, 013 (2007).

[81] P.A. Čerenkov, Dokl. Akad. Nauk SSSR **2**, 451 (1934).

[82] O. Heaviside, Phil. Mag. **27**, 324 (1889); I.E. Tamm and I.M. Frank, Dokl. Akad. Nauk SSSR **14**, 107 (1937).

[83] D. Colladay and V.A. Kostelecký, Phys. Rev. D **55**, 6760 (1997).

[84] S.R. Coleman and S.L. Glashow, Phys. Rev. D **59**, l16008 (1999).

[85] F.W. Stecker and S.L. Glashow, Astropart. Phys. **16**, 97 (2001).

[86] T. Jacobson, S. Liberati, and D. Mattingly, Phys. Rev. D **67**, 124011 (2003).

[87] M.A. Hohensee, R. Lehnert, D.F. Phillips, and R.L. Walsworth, Phys. Rev. Lett. **102**, 170402 (2009).

[88] V.A. Kostelecký and M. Mewes, Phys. Rev. D **85**, 096005 (2012).

[89] V.A. Kostelecký and M. Mewes, Phys. Rev. D **88**, 096006 (2013).

[90] F. W. Stecker and S. T. Scully, New J. Phys. **11**, 085003 (2009).

[91] V.A. Kostelecký and S. Samuel, Phys. Rev. D **39**, 683 (1989).

[92] V.A. Kostelecký and R. Lehnert, Phys. Rev. D **63**, 065008 (2001).

[93] D. Colladay and P. McDonald, J. Math. Phys. **43**, 3554 (2002).

[94] F. Englert and R. Brout, Phys. Rev. Lett. **13**, 321 (1964).

[95] P. W. Higgs, Phys. Lett. **12**, 132 (1964).

[96] P. W. Higgs, Phys. Rev. Lett. **13**, 508 (1964).

[97] M. E. Peskin and D. V. Schroeder, An Introduction to Quantum Field Theory, Perseus, Reading, 1995.

[98] T. P. Cheng and L. F. Li, Gauge Theory of Elementary Particle Physics, Oxford University Press, Oxford, 1988.

[99] C. Giunti and C. W. Kim, Fundamentals of Neutrino Physics and Astrophysics, Oxford University Press, New York, 2007.

[100] P. Langacker, The Standard Model and Beyond, Taylor and Francis Group, Boca Raton, 2010.

[101] M. D Schwartz, Quantum Field Theory and the Standard Model, Cambridge University Press, New York, 2014.

[102] J. Montaño, H. Novales, et al., e-Print arXiv:2107.12444v1.

[103] W. Hollik, J. I. Illana, S. Rigolin, C. Schappacher, and D. Stckinger, Nucl. Phys. B **551**, 3 (1999).

[104] M. Nowakowski, E. A. Paschos, and J. M. Rodríguez, Eur. J. Phys. **26**, 545 (2005).

[105] C. Broggini, C. Giunti, and A. Studenikin, Adv. High Energy Phys. **2012**, 1 (2012).

[106] D. Colladay and P. McDonald, J. Math. Phys. **43**, 3554 (2002).

[107] G. Passarino and M. Veltman, Nucl. Phys. B **160**, 151 (1979).

[108] R. Mertig, M. Böhm, and A. Denner, Comput. Phys. Commun. **64**, 345 (1991).

[109] H. H. Patel, Comput. Phys. Commun. **197**, 276 (2015).

[110] C. G. Bollini and J. J. Giambiagi, Nuovo Cimento Soc. Ital. Fis. **12B**, 20 (1972).

[111] C. G. Bollini and J. J. Giambiagi, Nuovo Cim. B **12**, 20 (1972).

[112] G. 't Hooft and M. Veltman, Nucl. Phys. B **153**, 365 (1979).

[113] J. Schwinger, Phys. Rev. **73**, 416 (1948).

[114] T. Aoyama, M. Hayakawa, T. Kinoshita, and M. Nio, Phys. Rev. Lett. **109**, 111807 (2012).

[115] T. Aoyama, M. Hayakawa, T. Kinoshita, and M. Nio, Phys. Rev. Lett. **109**, 111808 (2012).

[116] G. W. Bennett et al., Phys. Rev. Lett. **92**, 161802 (2004).

[117] D. Hanneke, S. Fogwell, and G. Gabrielse, Phys. Rev. Lett. **100**, 120801 (2008).

[118] D. Hanneke, S. F. Hoogerheide, and G. Gabrielse, Phys. Rev. A **83**, 052122 (2011).

[119] B. Regan, E. Commins, C. Schmidt, and D. DeMille, Phys. Rev. Lett. **88**, 071805 (2002).

[120] J. J. Hudson, D. M. Kara, B. E. Sauer, M. R. Tarbutt, and E. A. Hinds, Nature **473**, 493 (2011).

[121] D. M. Kara, I. J. Smallman, J. J. Hudson, B. E. Sauer, M. R. Tarbutt, and E. A. Hinds, New J. Phys. **14**, 103051 (2012).

[122] J. Baron, et al. (ACME Collaboration), Science **343**, 269 (2014).

[123] M. Pospelov and A. Ritz, Phys. Rev. D **89**, 056006 (2014).

[124] G. W. Bennett, et al., Phys. Rev. D **80**, 052008 (2009).

[125] K. Inami, et al., Phys. Lett. B **551**, 16 (2003).

[126] A. I. Hernández-Juárez, J. Montaño, H. Novales-Sánchez, M. Salinas, J. J. Toscano, and O. Vázquez-Hernández, Phys. Rev. D **99**, 013002 (2019).

[127] L. V. Avdeev and M. Yu. Kalmykov, Phys. Lett. B **436**, 132 (1998).

[128] P. Gambino and A. Sirlin, Phys. Rev. D **49**, R1160 (1994).

[129] D. Binosi and V. Pascalutsa, J. Phys. G **36**, 045001 (2009).

[130] P.A. Zyla, et al. (Particle Data Group), Prog. Theor. Exp. Phys. **2020** (2020).

[131] G. Schneider, et al., Science **358**, 1081 (2017).

[132] P. J. Mohr, D. B. Newell, and B. N. Taylor, Rev. Mod. Phys. **88**, 035009 (2016).

[133] B. K. Sahoo, Phys. Rev. D **95**, 013002 (2017).

[134] C. Abel, et al., Phys. Rev. Lett. **124**, 081803 (2020).